An unconventional T cell nexus drives HCK-mediated chronic obstructive pulmonary disease in mice

Amy T. Hsu,[a] Robert J. J. O'Donoghue,[b,e] Evelyn Tsantikos,[a] Timothy A. Gottschalk,[a] Jessica G. Borger,[a] Nicholas A. Gherardin,[c] Calvin Xu,[c] Hui-Fern Koay,[c] Dale I. Godfrey,[c] Matthias Ernst,[b] Gary P. Anderson,[d] and Margaret L. Hibbs[a,*]

[a]Department of Immunology, School of Translational Medicine, Monash University, Melbourne, Victoria, 3004, Australia
[b]Olivia Newton-John Cancer Research Institute, La Trobe University School of Cancer Medicine, Heidelberg, Victoria, 3084, Australia
[c]Department of Microbiology and Immunology, Peter Doherty Institute for Infection and Immunity, The University of Melbourne, Parkville, Victoria, 3010, Australia
[d]Lung Health Research Centre, Department of Biochemistry and Pharmacology, The University of Melbourne, Parkville, Victoria, 3010, Australia

eBioMedicine
2025;115: 105707
Published Online 16 April 2025
https://doi.org/10.1016/j.ebiom.2025.105707

Summary

Background Chronic obstructive pulmonary disease (COPD) is a heterogeneous inflammatory lung disease leading to progressive, destructive lung function decline, disability and death, and it is refractory to all current treatments. Haematopoietic cell kinase (HCK) is a druggable SRC-family non-receptor protein tyrosine kinase and COPD candidate gene. It is implicated in the chronic and non-resolving inflammation that causes mucosecretory bronchitis and destruction of small airways and alveoli, but how it drives pathophysiology remains obscure.

Methods Studies primarily utilised gene-targeted mice with a gain-of-function mutation in *Hck* that rendered the enzyme constitutively active. Bone marrow chimeras were established to determine the origin of disease, and the lung disease was investigated using histopathology, morphometry, flow cytometry and single-cell sequencing techniques. Detailed pathways mediating disease pathogenesis were examined using specialised knockout mice.

Findings $Hck^{F/F}$ mice developed intense granulocytic mucosecretory inflammation. Bone marrow chimeras revealed that stromal-derived granulocyte-colony-stimulating factor (G-CSF) resulted in lung inflammation and emphysema but not mucus production; while its upstream regulator, interleukin (IL)-17A, itself implicated in emphysema and mucus overproduction, was produced by Vγ6Vδ1 T cells that were recruited to airspaces. Nonetheless, lung disease was unchanged upon genetic deletion of γδ T cells, due to niche-filling expansion of IL-17A-producing mucosal-associated invariant T cells. Strikingly, IL-17A deletion abrogated inflammation, alveolar destruction and mucus overproduction in $Hck^{F/F}$ lungs.

Interpretation These findings highlight the role of HCK as an apical regulator of an unconventional T cell axis that drives IL-17A/G-CSF/granulocyte-mediated pathology in COPD, and underscore the rationale for therapeutically targeting HCK.

Funding This work received support from the National Health and Medical Research Council Australia, the Victorian Cancer Agency, Melbourne Australia, the Australian Research Council, the Australian Government and the School of Translational Medicine, Monash University, Australia.

Keywords: Constitutive HCK activation; Chronic obstructive pulmonary disease; Mucus-producing goblet cells; IL-17A/G-CSF axis; Granulocytes; Unconventional T cells

Introduction

Chronic obstructive pulmonary disease (COPD) afflicts around 480 million people, causes over 3.3 million deaths and is a major cause of hospitalisation and disability globally.[1] COPD is defined by clinical history and lung function decline below the forced expiratory volume in 1 s/forced vital capacity ratio of 0.7. Pathophysiologically, lung function decline is caused by

*Corresponding author.
E-mail address: Margaret.Hibbs@monash.edu (M.L. Hibbs).
[e]Present address: 360biolabs, Melbourne, Victoria 3004, Australia.

Research in context

Evidence before this study

HCK is a myeloid-selective SRC-family kinase with strong links to chronic obstructive pulmonary disease both experimentally and clinically. A recent clinical study has revealed the devastating consequences of constitutive activation of this enzyme, with myeloid cell activation resulting in treatment-unresponsive fatal respiratory disease. However, exactly how HCK might drive lung disease pathogenesis is not known.

Added value of this study

We employed a physiologically relevant mouse model of constitutively active HCK to investigate mechanisms underlying lung disease. Using sophisticated bone marrow chimera studies, we defined the main cellular sources of disease mediators, and by utilising specialised knockout mice we uncovered a niche dynamic between two key IL-17A-producing unconventional T cell types that ultimately led to the identification of IL-17 as a major driver of immunopathology. Complete genetic ablation of IL-17 preserved lung structure and protected mice from severe mucosecretory emphysematous lung disease.

Implications of all the available evidence

Our study represents a major step towards understanding how augmented HCK activity drives lung disease. These findings identify HCK as an important therapeutic target at the apex of an IL-17A/G-CSF/granulocyte and unconventional T cell pathogenic axis that offers improved insights into the fundamental pathobiology of chronic obstructive pulmonary disease. Given the druggable nature of HCK, inhibitors of this enzyme, or its downstream mediators, should be explored as a therapeutic strategy in distinct endotypes of chronic obstructive pulmonary disease.

chronic, non-resolving lung inflammation that destroys small airways (bronchiolitis) and alveoli (emphysema). It also triggers excessive viscid mucus secretion (bronchitis) and small airway mucus plugging, which are directly associated with decline in lung function, morbidity and mortality.[2] This prominent inflammation comprises infiltrating macrophages, neutrophils and lymphocytes and is linked to tissue damage. Neutrophils are highly implicated in COPD as their products stimulate mucus gene expression, goblet cell metaplasia, and promote alveolar tissue destruction.[3–7] However, conventional anti-inflammatory drugs, including glucocorticosteroids, have little effect on the neutrophilic inflammation that predominates in COPD and are not effective at slowing disease progression.[8] There is, accordingly, a pressing need for further insights into the fundamental molecular and cellular mechanisms of this disease in order to develop disease modifying therapies.

Haematopoietic cell kinase (HCK) is a non-receptor SRC-family tyrosine kinase signalling intermediate that regulates the activity of myeloid cells,[9] and is thus a candidate COPD gene. Indeed, human genetic studies have revealed that *HCK* polymorphisms, which increase HCK activity by increasing protein levels, are prominent in COPD.[10–12] Recently, an individual was identified that harboured a *de novo* mutation in *HCK* that resulted in loss of its inhibitory tyrosine residue, triggering augmented HCK activity in myeloid cells.[13] This caused early-onset pulmonary inflammation that was poorly responsive to glucocorticoid treatment and immunosuppressive therapies, leading ultimately to fatal respiratory failure, and highlighted an unmet need to better understand the processes underlying HCK-mediated disease.[13] In contrast to many known COPD candidate genes which are difficult to modify, the kinase domain of HCK is "druggable" and can be inhibited with small molecules.[14] However, exactly how HCK might drive the pathogenesis of COPD is not known, but further understanding of disease mechanisms may provide rationale for specific HCK inhibitors to treat pulmonary inflammation.

To better understand the pathobiology of HCK in COPD, we studied a mouse model where HCK has been constitutively activated by introducing a gene-targeted gain-of-function mutation in the kinase regulatory region, where a regulatory tyrosine (Y) residue has been mutated to a phenylalanine (F), mimicking clinical observations. Homozygous $Hck^{F/F}$ mice exhibit enhanced myeloid cell activity and spontaneously develop myeloid-rich lung inflammation, which drives emphysema and marked increases in goblet cells,[15,16] the latter being the root cause of chronic bronchitis and mucus plugging. Thus, this model closely resembles clinical disease. Herein, we show that $Hck^{F/F}$ mice display marked upregulation of the proinflammatory cytokine IL-17A that is prominent in COPD,[17] and G-CSF/colony-stimulating factor 3 (CSF3), a haematopoietic growth factor produced by pulmonary epithelial and endothelial cells that is critical for the development, survival, mobilisation and priming of myelomonocytic cells[18] and is implicated as a determinant of COPD and its complex comorbidome.[19] By probing the cellular source of IL-17 in $Hck^{F/F}$ mice, we further uncover a reciprocally cross-regulating cellular axis of IL-17-producing unconventional γδ T cells and mucosal-associated invariant T (MAIT) cells. These findings further underscore the unappreciated importance of HCK in the molecular and cellular pathogenesis of COPD and suggest the therapeutic utility of targeting this candidate disease axis. Furthermore, these insights will allow the identification of patient endotypes most likely to respond to HCK inhibitors.

Methods

Mice

C57BL/6 background $Hck^{F/F}$ mice (129T1/Sv-*Hck*^{tm1ern}/LudApb; denoted as FF in figures),[15,16] were obtained from the Ludwig Institute for Cancer Research, Australia under a Material Transfer Agreement (Australian Phenome Bank ID 5490). T cell receptor (TCR) δ chain-deficient ($Tcrd^{-/-}$) mice (RRID:IMSR_JAX:002120),[20] and $Il17a^{-/-}$ mice[21] (obtained from the Tokyo University of Science, Tokyo, Japan under a Material Transfer Agreement) were on a C57BL/6 background. C57BL/6 mice (denoted as B6 in figures) were used as controls for all studies. Mice were housed under standard 12-h light–dark conditions and had unlimited access to food and water. Animals were examined prior to the initiation of an experiment and any that appeared unwell were excluded, with weight loss, facial expression and activity level used as key exclusion criteria. $Hck^{F/F}Tcrd^{-/-}$ mice and $Hck^{F/F}Il17a^{-/-}$ mice were generated to examine the role of γδ T cells and IL-17A in lung disease. $Csf3^{-/-}$ mice (RRID:IMSR_JAX:002398),[22,23] obtained from the Ludwig Institute for Cancer Research under a Material Transfer Agreement, were used as recipients in bone marrow (BM) chimera experiments. The genotype of animals was confirmed by PCR analysis of tail DNA (Supplementary Table S1), and mice were age and sex matched, using appropriately-matched genetic background controls. No specific algorithm was used to match mice; whole litters generally matched for sex were used, and control C57BL/6 mice were then selected on the basis of the mutants used, matching for age and sex. Supplementary File 1 contains information on the sex of the mice used for the individual components of the study.

Ethics

Animal experiments were approved by the Animal Ethics Committees of the Alfred Research Alliance, the University of Melbourne, and the Olivia Newton-John Cancer Research Institute (Approval numbers: E1688/2016/M; E1830/2018/M; E8248/2021/M; UoM #10077). Experiments adhered to National Health and Medical Research Council of Australia (NHMRC) guidelines, the ARRIVE guidelines, and the Australian Code for the Care and Use of Animals for Scientific Purposes.

Response to glucocorticosteroid treatment

To examine the response to glucocorticosteroid treatment, 10-wk-old $Hck^{F/F}$ mice were randomised and then treated daily for 4 weeks by intraperitoneal injection with phosphate-buffered saline (PBS) or 2 mg/kg dexamethasone (Product Number D2915, Sigma–Aldrich, Burlington, MA, USA). Dexamethasone has excellent bioavailability by the intraperitoneal route, and previous studies have shown that this dose and delivery method given for 7-days during the allergen challenge period limits eosinophilic asthma responses in mice.[24] Mice were then euthanised by sodium pentobarbitone overdose (541.67 mg/kg, Product code LETHA450, Virbac, Milperra, NSW, Australia) for assessment of immune cell composition in spleen and lung tissue.

Bone marrow chimeras

To ascertain the cell type responsible for the lung disease phenotypes in $Hck^{F/F}$ mice, bone marrow (BM) chimeras were established using the following combinations: C57BL/6 BM into C57BL/6 mice as a negative control (B6 > B6); $Hck^{F/F}$ BM into $Hck^{F/F}$ mice as a positive control (FF > FF); $Hck^{F/F}$ BM into C57BL/6 mice to assess whether $Hck^{F/F}$ BM could induce lung disease in control mice (FF > B6); and, C57BL/6 BM into $Hck^{F/F}$ mice to assess whether the lung environment in $Hck^{F/F}$ mice drives the phenotype (B6 > FF). In the second series of experiments, G-CSF-deficient recipients ($Csf3^{-/-}$; GKO) were used to determine the role of stromal-derived G-CSF in the lung disease phenotype by transplanting $Hck^{F/F}$ BM into C57BL/6 or $Csf3^{-/-}$ mice (FF > B6 and FF > GKO respectively). Briefly, BM was flushed aseptically from the femurs of donor mice, washed, filtered and resuspended in PBS. Recipient mice were lethally irradiated with two equal doses of 450 rad separated by 3 h using an X-ray irradiator (RS 2000, Rad Source Technologies, Buford, GA, USA). One hour after the second dose, recipient mice received 1×10^6 donor BM cells through lateral tail vein injection, and were then placed on oral antibiotics (enrofloxacin, Baytril 25, Bayer Australia Ltd, Pymble, NSW, Australia) during recovery for 3 weeks and housed on wood-chip bedding to expedite residential alveolar macrophage turnover.[25] G-CSF-deficient recipients ($Csf3^{-/-}$) were susceptible due to myelosuppression,[22] with 60% (9/15) of irradiated mice being euthanised by slow-fill CO_2 asphyxiation during the recovery period due to wasting. All other chimera combinations recovered fully. Reconstituted mice were then analysed 12–16 weeks post-irradiation.

Bronchoalveolar lavage and cytospins

Mice were terminally anaesthetised by intraperitoneal injection of 600 mg/kg sodium pentobarbitone. Bronchoalveolar lavage (BAL) was performed by washing the lungs with ice-cold PBS (4 × 400 μl) using a modified 21G-needle inserted in the trachea. Cell counts were performed using a haemocytometer. Cells were centrifuged onto glass slides (320 rpm, 7 min) using a Shandon Cytospin 3 (Thermo Fisher Scientific, Waltham, MA, USA) and then stained with Hemacolor Rapid Staining of Blood Smear staining kit (Product number 1.11661, Sigma–Aldrich). BAL fluid from the first wash was retained for cytokine measurement.

Lung fixation and histology

Lungs were inflation-fixed at 25-cm water pressure in 10% formalin (NBFG, Amber Scientific, Belmont, WA,

Australia) for at least 24 h, processed and then embedded in paraffin (Surgipath Paraplast Embedding Medium, Leica Biosystems, Mount Waverley, VIC, Australia). Whole lung sections were cut to a thickness of 4 μm, mounted onto SuperFrost Plus slides (J1800AMNZ, Menzel-Glaser/Epredia, Germany) and stained with Harris Haematoxylin (HH-1L, Amber Scientific) and 1% alcoholic eosin (EOS-1L, Amber Scientific) (H&E) for histopathology assessment. Slides of lung sections were also stained with 1% Alcian Blue (A5268-10G, Sigma–Aldrich)/1% Periodic Acid (PERI-500, Amber Scientific) and Schiff's Reagent (SCHF-500, Amber Scientific) followed by counterstaining with Harris Haematoxylin (HH-1L, Amber Scientific) (AB/PAS) for goblet cell analyses. H&E staining was performed at the Monash Histology Platform DIY facility and AB/PAS staining was performed by the Monash Histology Platform (Monash University, Clayton, VIC, Australia). AB/PAS-stained and H&E-stained lungs were scanned by the Monash Histology Platform using the Leica Aperio AT Turbo Brightfield slide scanner (Leica Biosystems, Nussloch, Germany) or captured on an Olympus BX-51 light microscope using 10×, 20× and 40× objectives (Olympus Australia, Notting Hill, VIC, Australia).

Morphometric analysis of lungs

The average size of alveolar airspaces was measured by the mean linear intercept (MLI) method.[26] Briefly, twenty equally distributed lines were drawn on H&E-stained lung cross-sections. The number of times each line intercepted with an alveolar wall was counted. The size of the alveolar airspace was then determined by dividing the known length of the line drawn across the images of the lung cross-sections (in μm) by the number of intercepts.

Goblet cell analysis

Goblet cell numbers were counted in high power field (HPF) images of the large airway.[27] Briefly, magenta-stained goblet cells in AB/PAS-stained lung cross-sections were counted at 400× magnification of images of the large airways and averaged across 10 random images of the large airways per lung.

Flow cytometry

Flow cytometry was used to discriminate the immune cell populations in BAL and digested lung tissue samples,[25] for analysis of lymphocyte populations in spleen[28] and for assessment of thymic development.[29,30] Single cell suspensions were incubated with Fc Block for 5–10 min (anti-mouse CD16/CD32, clone 2.4G2, BD Biosciences Catalogue # 553142, RRID: AB_394656), then stained with commercial anti-mouse monoclonal antibodies which are listed in Supplementary Table S2. Antibodies were first tested and validated by staining of single cell suspensions of mouse spleen or BAL. Technical data sheets with validation information are provided in the Reagent Validation file.

MAIT cells were detected using MR1-5-OP-RU tetramers,[31] and natural killer T (NKT) cells were detected using CD1d-α-GalCer tetramers.[32] Lung tissue NKT and MAIT cells were gated as $CD45^+CD11c^-B220^-CD3^{int}$CD1d-α-$GalCer^+$ and $CD45^+CD11c^-B220^-CD3^{int}$MR1-5-OP-$RU^+$ cells, respectively. MAIT cells were additionally assessed in the BAL and were gated as $CD45^+CD11c^-B220^-TCR\beta^+$ MR1-5-OP-RU^+. TCRβ was preferred over CD3 for the identification of NKT and MAIT cells; however, antibody usage was dependent upon availability at the time of the experiments. Innate lymphoid cells (ILC) were gated as $CD45^+$, $Lineage^-$ (TCR-β, B220, CD11c, CD11b negative), $CD127^+$. ILC1 were further gated as $Tbet^-ROR\gamma t^-NK1.1^+$; ILC2 as $ROR\gamma t^-$T-bet^+; and ILC3 as $Tbet^-ROR\gamma t^+$.

Intracellular staining for T-bet and RORγt was performed after fixation and permeabilisation of surface-stained cells using the Foxp3 Transcription Factor Staining Buffer Set (Catalogue number 00-5523-00, eBioscience, Waltham, MA, USA). Fluorescence Minus One (FMO) controls were used to aid in gating positive cells. Cytokine production was assessed by stimulating BAL or spleen cells with 50 ng/ml phorbol 12-myristate 13-acetate (PMA, Product number P8139, Merck, Sigma–Aldrich) and 1 μg/ml ionomycin (Product number 407950, Merck, Sigma–Aldrich) or vehicle in the presence of GolgiPlug (Catalogue number 555029, BD Biosciences, Franklin Lakes, NJ, USA) for 4 h at 37 °C. Cells were then surface stained, fixed and permeabilised using the BD Cytofix/Cytoperm Fixation/Permeabilisation Plus Kit (Catalogue number 555028, BD Biosciences) and stained for intracellular IL-17A and interferon-γ (IFN-γ). Stained cells were acquired on an LSRII or LSRFortessa X-20 (BD Biosciences), and data was analysed using FlowJo software (Version 10.10.0, FlowJo, LLC, Ashland, OR, USA). Doublets were excluded using forward scatter area (FSC-A) vs forward scatter height (FCS-H) gating, and dead cells were excluded using FluoroGold staining at a 1:1000 final dilution in the antibody cocktail (Catalogue number sc-358883, Santa Cruz Biotechnology, Dallas, TX, USA). Gating strategies for BAL and lung tissue are shown in Supplementary Figures S1 and Figure S2 respectively.

Cell sorting

Single $CD3^{high}$ and $CD3^{low}$ γδ T cells were sorted from mouse spleen and digested lung tissue; and B cells, CD4+, CD8+ and γδ T cells were sorted from mouse spleen using a BD FACSAria (Beckton Dickinson). Doublets were omitted based on FSC-A vs FSC-H gating, and dead cells were excluded using fluorogold staining. γδ T cells in the spleen were defined as $CD3^{high}$ or $CD3^{low}$ and were $CD45^+B220^-\gamma\delta TCR^+$. B cells in the spleen were defined as $CD45^+B220^+$; $CD4^+$ T cells were $B220^-CD3^+CD4^+$; and $CD8^+$ T cells were

$B220^{-}CD3^{+}CD8^{+}$. γδ T cells in the lung were defined as $CD3^{high}$ or $CD3^{low}$ and were $CD45^{+}CD11c^{-}B220^{-}CD4^{-}CD8^{-}\gamma\delta TCR^{+}$.

Single cell PCR and γδ TCR sequencing

TCR-γ and TCR-δ transcripts were amplified from single $CD3^{high}$ or $CD3^{low}$ γδ T cells sorted into plates as described.[33] Briefly, complementary DNA was generated from RNA extracted from the sorted cells and amplified by two rounds of PCR with primers designed against respective γδTCR regions.[34] PCR products were separated by gel electrophoresis and sequenced as described.[35] Successfully amplified TCR genes as determined by agarose gel electrophoresis were subjected to Sanger Sequencing using internal TCR delta chain (5′-GATGACAATAGCAGGATCAAAC-3′) or TCR gamma chain (5′-CCCAGAATCGTGTTGCT-3′) primers at Australian Genome Research Facility (AGRF), Melbourne. Sequence data was analysed using IMGT V-QUEST sequence alignment software v3.4.17.

Cytokine measurement in BAL fluid

Cytokine levels in BAL fluid were measured using a Luminex multiplex assay (R&D Systems, Minneapolis, MN, USA) following the manufacturer's instructions. IL-17A levels in BAL fluid were quantified using a mouse IL-17A ELISA kit (DY421-05, R&D Systems).

RNA extraction and quantitative reverse transcription PCR (qRT-PCR)

Gene expression of *Hck* was assessed in cells sorted from mouse spleen (B cells, CD4+, CD8+ and γδ T cells) by qPCR. Briefly, RNA was extracted from sorted cells using the RNeasy Mini Kit (Catalogue number 73404, Qiagen, Hilden, Germany) and cDNA was synthesised with the High-Capacity RNA-to-cDNA kit (Catalogue number 4387406, Applied Biosystems, Thermo Fisher Scientific), both according to the manufacturer's instructions. Gene expression was assessed using Taqman validated primer sets against mouse *Hck* (Mm01241463_m1, Applied Biosystems, Thermo Fisher Scientific) and mouse *Rn18s* (Mm04277571_s1, Applied Biosystems, Thermo Fisher Scientific), and fold change was calculated relative to *Rn18s*. Three independent experiments were conducted and the data in each experiment was normalised by expressing the fold difference relative to mouse γδ T cells, allowing data to be pooled.

For lung gene expression, the middle right lobe of mouse lung was collected for qPCR and RNA was isolated using the TRIzol method with tissue homogenised using the Qiagen TissueLyser II (Qiagen) and 3 mm tungsten carbide beads (Qiagen).[36] RNA was converted to cDNA using the FIREScript RT cDNA synthesis kit (Catalogue number 06-15-00200, Solis BioDyne, Tartu, Estonia). PowerUp SYBR Green Master Mix (Catalogue number A25778, Thermo Fisher Scientific) was used to perform qRT-PCR, with genes of interest assessed using validated self-designed primers and published primer sequences (Supplementary Table S3). Genes were amplified on a QuantStudio Flex 5 (Thermo Fisher Scientific) and CT values acquired. The relative expression of each target gene was calculated by the $2^{-\Delta\Delta}$CT method and was normalised to ribosomal *18s* expression.

Statistics

Data is presented as median ± interquartile range (IQR), unless otherwise specified. Since lung disease can be patchy and irregular, and flow cytometry data can be variable, an assumption was made that the data was not normally distributed, and additionally, in some cases, sample sizes were small, so nonparametric tests were used for statistical analyses. For morphometric and goblet cell analyses, investigators were blinded to experimental groups during analyses. For bone marrow chimera experiments, mice were randomly assigned to be either donors or recipients. Sizes of experimental groups were based on power calculations. In general, we used at least 5 mice per group based on an 80% confidence of detecting a 10% difference between means where the standard deviation was 20% of the mean. Where the standard deviation was determined to be greater (15% difference between means) we used 10 mice per group. Samples were collected across multiple experiments and study endpoints. Where multiple experiments were performed to achieve the correct sample size, the data was pooled, summed and expressed as median ± IQR as a robust measure of central tendency and spread. The ROUT outlier method (GraphPad Prism Software version 9.0.1, Boston, MA, USA) was used to detect outliers in the data, and a few qPCR and flow cytometry data points were excluded from the dataset on this basis. Other exclusions included samples where BAL was not satisfactorily retrieved, and flow cytometry samples where staining was not successful. For comparisons of two groups, the non-parametric Mann–Whitney U test was used, and for three or more groups, Kruskal–Wallis test with Dunn's post-test was used. Analyses were performed using GraphPad Prism software. Significance is shown by asterisks, with *P*-value <0.05 considered significant. All statistical data is presented in Supplementary File 1 under tabs corresponding to each figure. Supplementary File 1 also includes information on the numbers of mice used in the individual components of the study (numbers of mice analysed), together with information on the sex distribution of the mice analysed (sex of mice analysed). The mouse numbers analysed are also indicated in each of the figure legends and in the figure panels, and each data point represents a single mouse.

Role of funders

Funders had no role in the study design, data collection, analysis and interpretation, nor in the writing of this manuscript.

Results

Hck$^{F/F}$ mice exhibit increased goblet cell numbers in large airways and emphysema

We have previously reported that adult Hck$^{F/F}$ mice develop lung inflammation and increased numbers of mucus-producing goblet cells in conducting airways.[15] To further understand the genesis of this phenotype, we examined the lungs of juvenile and young adult mice (Fig. 1a and b). Quantification of AB/PAS-stained lung tissue cross-sections showed a marked increase in goblet cell numbers in the large conducting airways of 4-wk-old Hck$^{F/F}$ mice (Fig. 1c left panel, $P < 0.01$, Mann–Whitney U test), which persisted in the large airways of older mice (Fig. 1c right panel, $P < 0.01$, Mann–Whitney U test). Goblet cells were not apparent in small airways of Hck$^{F/F}$ mice of any age.

Gene expression analyses revealed that the mucin genes *Muc5ac, Muc5b* and *Muc1* were significantly increased in the lungs of 4-wk-old Hck$^{F/F}$ mice (Fig. 1d left panel, $P < 0.01$ for *Muc5ac* and *Muc5b*, $P < 0.05$ for *Muc1*, Mann–Whitney U test), consistent with the presence of increased goblet cells, while upregulated *Muc5ac* and *Muc1* persisted at 12 weeks of age (Fig. 1d right panel, $P < 0.05$ for *Muc5a*, $P < 0.01$ for *Muc1*, Mann–Whitney U test). Thus, Hck$^{F/F}$ mice develop sustained mucus overproduction, which is a trait consistently associated with disease morbidity and lung function decline in COPD.[2] Consistent with clinical findings linking mucus overproduction to a more aggressive disease course,[37] histopathology showed lung tissue damage (Fig. 1e) and morphometric analyses demonstrated significantly enlarged alveolar airspaces in 12-wk-old Hck$^{F/F}$ mice ($P < 0.01$, Mann–Whitney U test) relative to 4-wk-old mice (Fig. 1f, $P = 0.3434$, Mann–Whitney U test). Inflammatory cell infiltration into the lungs was also evident in both 4- and 12-wk-old Hck$^{F/F}$ mice (Fig. 1e).

Hck$^{F/F}$ mice exhibit myeloid-rich lung inflammation

To investigate the cellular landscape in the inflamed lung, immune cells from 4- to 12-wk-old mice were examined by cytology (Fig. 2a), flow cytometry of BAL (Supplementary Figure S1), and lung tissue (Supplementary Figure S2). BAL cytospins prepared from 4- and 12-wk-old control mice contained only small alveolar macrophages, with quiescent morphology, typical of uninflamed lungs (Fig. 2a). Contrastingly, alveolar macrophages from matched Hck$^{F/F}$ mice were enlarged and vacuolated, consistent with activation, and the BAL contained other immune cells (Fig. 2a), particularly neutrophils, which are linked with mucus hypersecretion and glucocorticosteroid unresponsiveness,[38] and eosinophils, which are associated with more frequent COPD exacerbations.[39] BAL cell counts were significantly elevated in 4-wk-old Hck$^{F/F}$ mice (Fig. 2b top panel, $P < 0.0001$, Mann–Whitney U test), demonstrating early-onset pulmonary inflammation, and remained elevated in 12-wk-old Hck$^{F/F}$ mice (Fig. 2b bottom panel, $P < 0.0001$, Mann–Whitney U test).

Flow cytometry of BAL revealed that 4-wk-old C57BL/6 mice had >99% CD45^{+}CD11c^{+} alveolar macrophages while Hck$^{F/F}$ mice had a high proportion of CD45^{+}CD11c^{-} cells (Fig. 2c). Further analyses revealed that Hck$^{F/F}$ mice had markedly increased numbers of myeloid and lymphoid cells in BAL (Fig. 2d, $P < 0.01$ for alveolar macrophages, monocytes, neutrophils, eosinophils, CD4^{+} and CD8^{+} T cells, Mann–Whitney U test). Myeloid cells were also increased in lung tissue (Fig. 2e, $P < 0.001$ for alveolar macrophages, $P = 0.095$ for neutrophils and $P < 0.0001$ for eosinophils, Mann–Whitney U test), while CD4^{+} and CD8^{+} T cells were not expanded (Fig. 2e, $P > 0.1$, Mann–Whitney U test). Similarly enhanced myeloid-rich inflammation in the BAL ($P < 0.01$ for alveolar macrophages, neutrophils and eosinophils, Mann–Whitney U test) and lungs ($P < 0.05$ for alveolar macrophages, $P < 0.01$ for neutrophils and $P < 0.0001$ for eosinophils, Mann–Whitney U test) was noted in 12-wk-old Hck$^{F/F}$ mice (Fig. 2b and Supplementary Figure S3).

Gene expression analyses revealed that *Csf3*, which encodes the neutrophil growth and survival factor G-CSF[18]; the gene encoding IL-17A (*Il17a*), a pro-inflammatory cytokine upstream of G-CSF[40]; and the gene encoding IL-6 (*Il6*), which stimulates mucus production through an IL-17 axis,[41] were upregulated in 4-wk-old Hck$^{F/F}$ lung, correlating with neutrophilic inflammation (Fig. 2f, $P < 0.05$, Mann–Whitney U test). Expression of *Mmp12*, which encodes macrophage metalloelastase directly linked to human emphysema,[42] was mildly increased in 4-wk-old Hck$^{F/F}$ mice (Fig. 2f, $P < 0.05$, Mann–Whitney U test), but markedly upregulated in 12-wk-old Hck$^{F/F}$ mice (Fig. 2f, $P < 0.0001$, Mann–Whitney U test), correlating with the appearance of emphysema (Fig. 1e). When male and female mice were examined to determine if there was a sex bias in disease, no major sex differences in pulmonary inflammation or lung disease traits were noted (Supplementary Figure S4).

Since steroids are widely used to treat inflammatory lung diseases, the effect of corticosteroid treatment on lung inflammation in Hck$^{F/F}$ mice was assessed. Administration of high-dose 2 mg/kg dexamethasone (Dex) daily for 4-weeks suppressed numbers of B and T lymphocytes in the spleen of Hck$^{F/F}$ mice (Fig. 2g, $P < 0.01$ for B cells, $P < 0.05$ for T cells, Mann–Whitney U test), consistent with attaining pharmacodynamically effective systemic levels of glucocorticosteroid. However, dexamethasone had no effect on numbers of alveolar macrophages ($P = 0.7302$, Mann–Whitney U test) or inflammatory neutrophils in BAL ($P = 0.1111$, Mann–Whitney U test), and strikingly, it did not reduce numbers of eosinophils ($P = 0.1429$, Mann–Whitney U test) or CD4^{+} T cells ($P = 0.1905$,

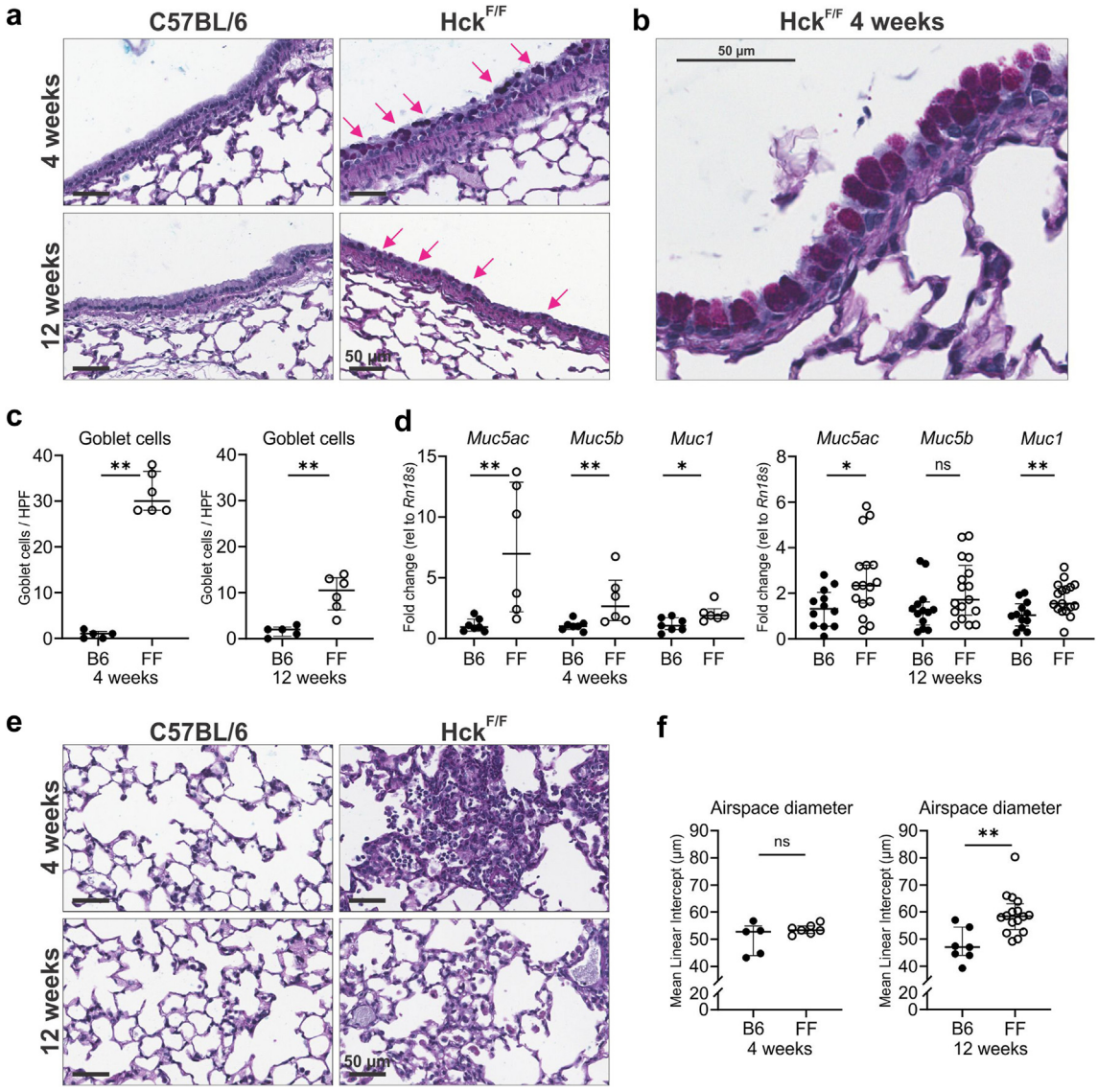

***Fig. 1:* Hck$^{F/F}$ mice exhibit early-onset increases in goblet cells and lung tissue destruction**. (**a**) Representative images of large airways of AB/PAS-stained lung cross-sections in 4- and 12-wk-old mice depicting mucus-producing goblet cells (arrows) in large airways of Hck$^{F/F}$ mice, scale bars represent 50 µm, (**b**) enlarged image of an independent 4-week-old Hck$^{F/F}$ mouse to highlight goblet cell morphology in conducting airway, scale bar represents 50 µm; and, (**c**) quantitation of goblet cells per high power field (HPF) in large airways, n = 5 B6 and 6 FF mice per group. (**d**) Lung gene expression analysis of *Muc5ac*, *Muc5b* and *Muc1* in 4-wk-old mice (n = 7 B6 and 6 FF mice) and 12-wk-old mice (n = 12 B6 and 17 FF mice). (**e**) Representative images of PAS/AB-stained lung cross-sections from 4- and 12-wk-old C57BL/6 and Hck$^{F/F}$ mice, scale bars represent 50 µm; and, (**f**) quantification of alveolar airspace size by mean linear intercept in 4-wk-old mice (n = 5 B6 and 7 FF mice) and 12-wk-old mice (n = 7 B6 and 16 FF mice). B6 = C57BL/6, FF = Hck$^{F/F}$. Data presented as median ± IQR. ns, not significant, $^{*}P < 0.05$, $^{**}P < 0.01$ (Mann–Whitney U test).

Mann–Whitney U test) in BAL (Fig. 2g). Histopathology of lung tissue confirmed that the increased number of goblet cells in Hck$^{F/F}$ mice was also steroid-insensitive (Supplementary Figure S5). Collectively, these data show that constitutive HCK activation promotes early-onset myeloid-rich lung inflammation that is refractory to corticosteroid therapy, indicating that Hck$^{F/F}$ mice are a model of corticosteroid-insensitive obstructive airways disease.

HCK activity in haematopoietic cells drives lung inflammation in Hck$^{F/F}$ mice

HCK is largely expressed by haematopoietic cells but it has also been observed in alveolar type II epithelial cells

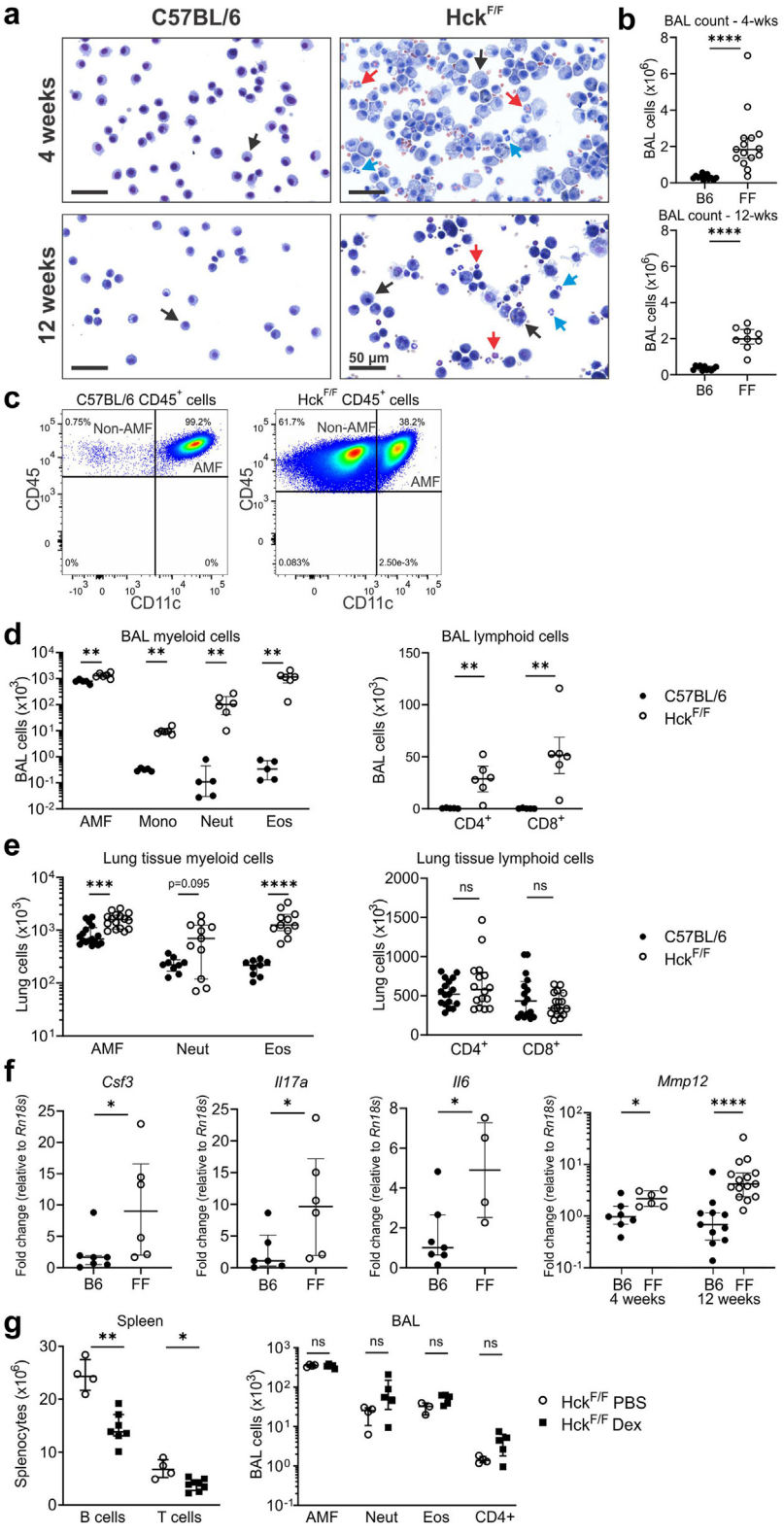

***Fig. 2:* Hck$^{F/F}$ mice display steroid-insensitive lung inflammation**. (**a**) Morphology of BAL cells from 4- and 12-wk-old C57BL/6 and Hck$^{F/F}$ mice, scale bars represent 50 µm. Black arrows, alveolar macrophages; red arrows, eosinophils; blue arrows, neutrophils. (**b**) BAL cell counts of

(Human Protein Atlas).[43] To determine the origin of lung disease in $Hck^{F/F}$ mice, BM chimeras were established. BAL cell cytology revealed that chimeras generated by transplanting $Hck^{F/F}$ BM into recipient C57BL/6 mice (FF > B6) had inflammation in alveolar airspaces similar to chimeras generated by transplantation of $Hck^{F/F}$ BM into recipient $Hck^{F/F}$ mice (FF > FF) (Fig. 3a), with elevated BAL cell counts compared to B6 > B6 controls (Fig. 3b, $P < 0.01$ for FF > B6 and $P < 0.05$ for FF > FF, Kruskal–Wallis test with Dunn's post-test). Chimeras generated by transplanting C57BL/6 BM into recipient $Hck^{F/F}$ mice (B6 > FF) displayed normal BAL cell counts (Fig. 3b); however, their alveolar macrophages exhibited a slightly activated morphology (Fig. 3a), likely due to a residual effect in the $Hck^{F/F}$ recipient lung environment. Flow cytometry revealed that the BAL of FF > B6 chimeras was inflamed like that of FF > FF mice, with increases in alveolar macrophages, neutrophils, eosinophils and T cells compared to B6 > B6 controls ($P < 0.05$ for alveolar macrophages, $P < 0.01$ for neutrophils, $P < 0.01$ for eosinophils and $P < 0.05$ for T cells, Kruskal–Wallis test with Dunn's post-test), while the BAL of B6 > FF chimeras contained only alveolar macrophages like control B6 > B6 chimeras (Fig. 3c). This data indicates that constitutively activated HCK within haematopoietic cells is sufficient to induce myeloid-rich lung inflammation.

Histological assessment of the large airways revealed that FF > B6 chimeras exhibited increased numbers of goblet cells compared to B6 > B6 controls (Fig. 3d), which was confirmed by quantitation (Fig. 3e, $P < 0.01$ Kruskal–Wallis test with Dunn's post-test), with numbers of goblet cells increased similarly to FF > FF chimeras (Fig. 3e, $P < 0.05$, Kruskal–Wallis test with Dunn's post-test), indicating that this trait is driven by $Hck^{F/F}$ BM. No changes in goblet cell numbers were observed in B6 > FF chimeras, indicating its resolution in the absence of $Hck^{F/F}$ BM (Fig. 3d and e). Morphometric measurements revealed that alveolar airspace size in B6 > FF BM chimeras was similar to that of control B6 > B6 chimeras (Fig. 3f). However, airspace size was enlarged in FF > B6 chimeras compared to B6 > B6 controls (Fig. 3f, $P < 0.05$, Kruskal–Wallis test with Dunn's post-test) and comparable to the increase seen in FF > FF BM chimeras (Fig. 3f, $P < 0.01$, Kruskal–Wallis test with Dunn's post-test), demonstrating that alveolar airspace damage is driven by $Hck^{F/F}$ BM. These data reveal that HCK activity in haematopoietic cells gives rise to lung inflammation, emphysema, and increased numbers of goblet cells.

Stromal-derived G-CSF promotes inflammation and emphysema in $Hck^{F/F}$ mice but not goblet cell changes

Since lung inflammation in $Hck^{F/F}$ mice is highly neutrophilic (Fig. 2d, $P < 0.01$, Mann–Whitney U test) and increased *Csf3* was observed in lung tissue (Fig. 2f, $P < 0.05$, Mann–Whitney U test), the source of G-CSF was investigated using BM chimeras and $Csf3^{-/-}$ mice as recipients. Chimeras generated by transplanting $Hck^{F/F}$ BM into $Csf3^{-/-}$ recipients (FF > GKO) showed that loss of stromal-derived G-CSF markedly limited lung inflammation, with fewer inflammatory cells in BAL cytospins (Fig. 4a) and lower BAL cell count compared to chimeras where $Hck^{F/F}$ BM was transplanted into C57BL/6 recipients (FF > B6) (Fig. 4b, $P < 0.01$, Kruskal–Wallis test with Dunn's post-test). Flow cytometry of BAL revealed that FF > GKO chimeras had fewer alveolar macrophages, neutrophils and eosinophils compared to FF > B6 chimeras (Fig. 4c, $P < 0.01$ for alveolar macrophages, $P < 0.05$ for neutrophils and $P = 0.0595$ for eosinophils, Kruskal–Wallis test with Dunn's post-test), while $CD3^+$ T cell counts remained elevated (Fig. 4c, $P > 0.9999$, Kruskal–Wallis test with Dunn's post-test). Screening of BAL fluid showed that naive $Hck^{F/F}$ mice had elevated protein levels of CXCL2 ($P < 0.01$), IL-6 ($P < 0.01$), MMP-9 ($P < 0.01$), G-CSF ($P < 0.01$), and IL-17A ($P < 0.05$), compared to the BAL fluid from FF > GKO chimeras (Fig. 4d, Mann–Whitney U test).

The reduction of inflammatory cells and proteins in the lungs of FF > GKO chimeras suggested that $Hck^{F/F}$ BM was not capable of inducing inflammation and lung disease in a G-CSF-deficient environment. This was revealed by lung histopathology (Fig. 4e) and confirmed by morphometry, which showed that while emphysema was present in FF > B6 chimeras (Fig. 4f, $P < 0.05$, Kruskal–Wallis test with Dunn's post-test), emphysema did not develop in FF > GKO chimeras (Fig. 4f, $P = 0.9512$, Kruskal–Wallis test with Dunn's post-test). Despite less inflammation and emphysema in FF > GKO chimeras, goblet cells were still present in the large airways, albeit with a different mucus staining pattern (Fig. 4g), and there were more goblet cells per

4-wk-old (n = 13 B6 and 15 FF mice) and 12-wk-old mice (n = 11 B6 and 9 FF mice). (**c**) Representative flow cytometry pseudocolour plots depicting all viable $CD45^+$ cells in the BAL of 4-wk-old C57BL/6 and $Hck^{F/F}$ mice. Flow cytometric quantitation of myeloid and lymphoid cells in (**d**) BAL (n = 5 B6 and 6 FF mice) and (**e**) lung tissue (n = 17 B6 and 16 FF mice for alveolar macrophages and lymphoid cells, n = 9 B6 and 11 FF mice for neutrophils and eosinophils) from 4-wk-old mice; AMF, alveolar macrophages; Mono, monocytes; Neut, neutrophils; Eos, eosinophils. (**f**) Inflammatory gene expression in lung tissue of 4-wk-old mice (n = 7 B6 and 4–6 FF mice); *Mmp12* expression in 4-wk-old (n = 7 B6 and 6 FF mice) and 12-wk-old mice (n = 12 B6 and 16 FF mice). (**g**) $Hck^{F/F}$ mice were treated for 4 weeks with PBS (n = 3–4) or 2 mg/kg dexamethasone (Dex) (n = 8) and corticosteroid sensitivity was assessed by analysis of cell populations in spleen (n = 7–8) and BAL (n = 5) by flow cytometry. B6 = C57BL/6, FF = $Hck^{F/F}$. Data presented as median ± IQR. ns, not significant; $^*P < 0.05$, $^{**}P < 0.01$, $^{***}P < 0.001$, $^{****}P < 0.0001$ (Mann–Whitney U test).

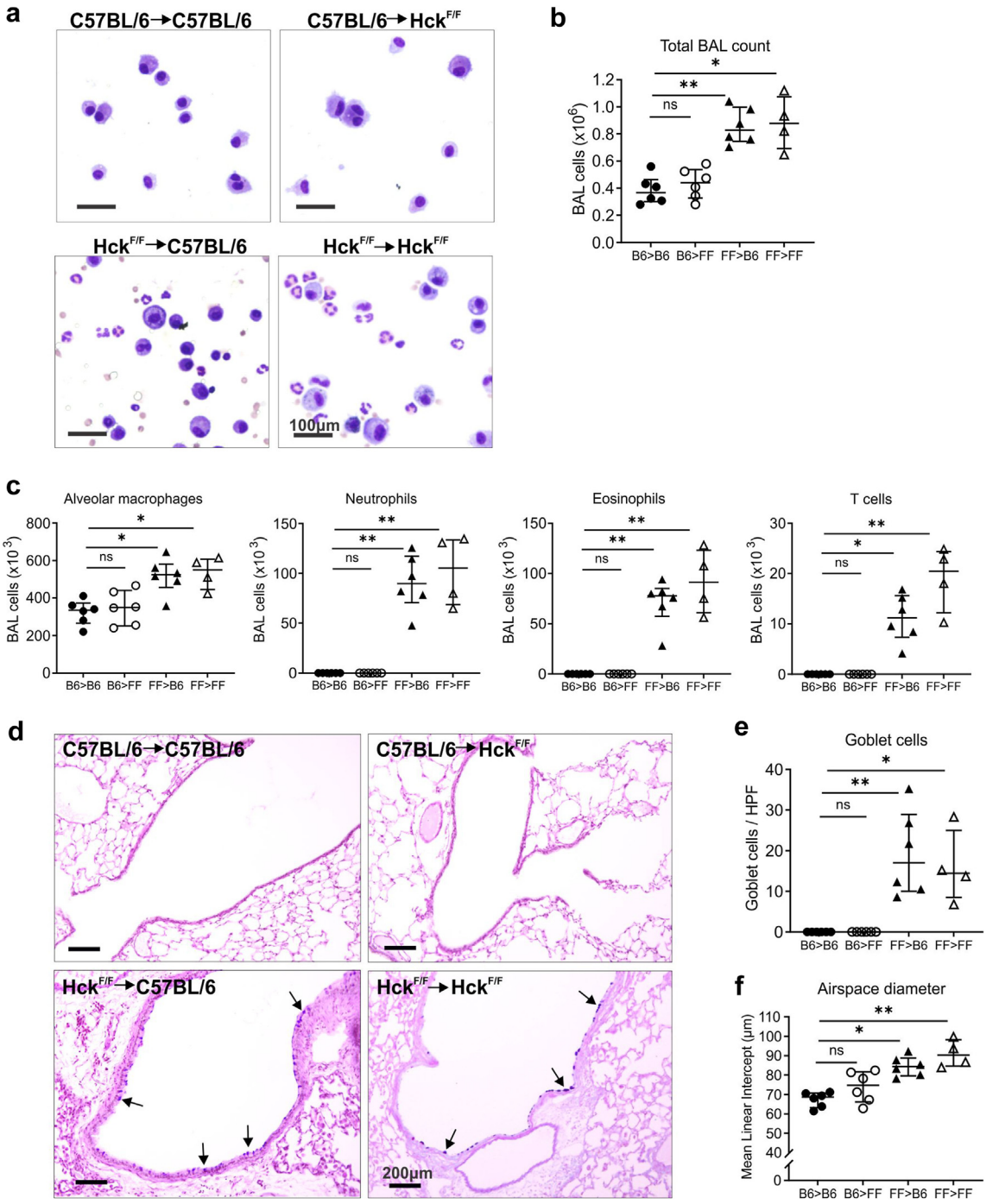

***Fig. 3:* Hck$^{F/F}$ haematopoietic cells drive lung inflammation, emphysema and increases in goblet cells**. BM chimeras were established as follows: B6 > B6 and B6 > FF denotes C57BL/6 BM transplanted into C57BL/6 or Hck$^{F/F}$ mice respectively, FF > B6 and FF > FF denotes Hck$^{F/F}$ BM transplanted into C57BL/6 or Hck$^{F/F}$ mice respectively. BM chimeras were analysed 16 weeks post-transplantation, n = 6 mice per group except for FF > FF, where n = 4. (**a**) Morphological analysis of BAL cells, scale bars represent 100 µm; and, (**b**) total BAL counts of BM chimeras. (**c**) Flow cytometric quantitation of immune cells in BAL from indicated BM chimeras. (**d**) Representative AB/PAS-stained lung cross-sections through large airways of the indicated BM chimeras depicting mucus-producing goblet cells (arrows), scale bars represent 200 µm. (**e**) Quantification of goblet cells numbers in AB/PAS-stained lungs and (**f**) alveolar diameter by mean linear intercept analysis of H&E-stained lungs. Data presented as median ± IQR. Ns, not significant; *P < 0.05, **P < 0.01 (Kruskal–Wallis test with Dunn's post-test).

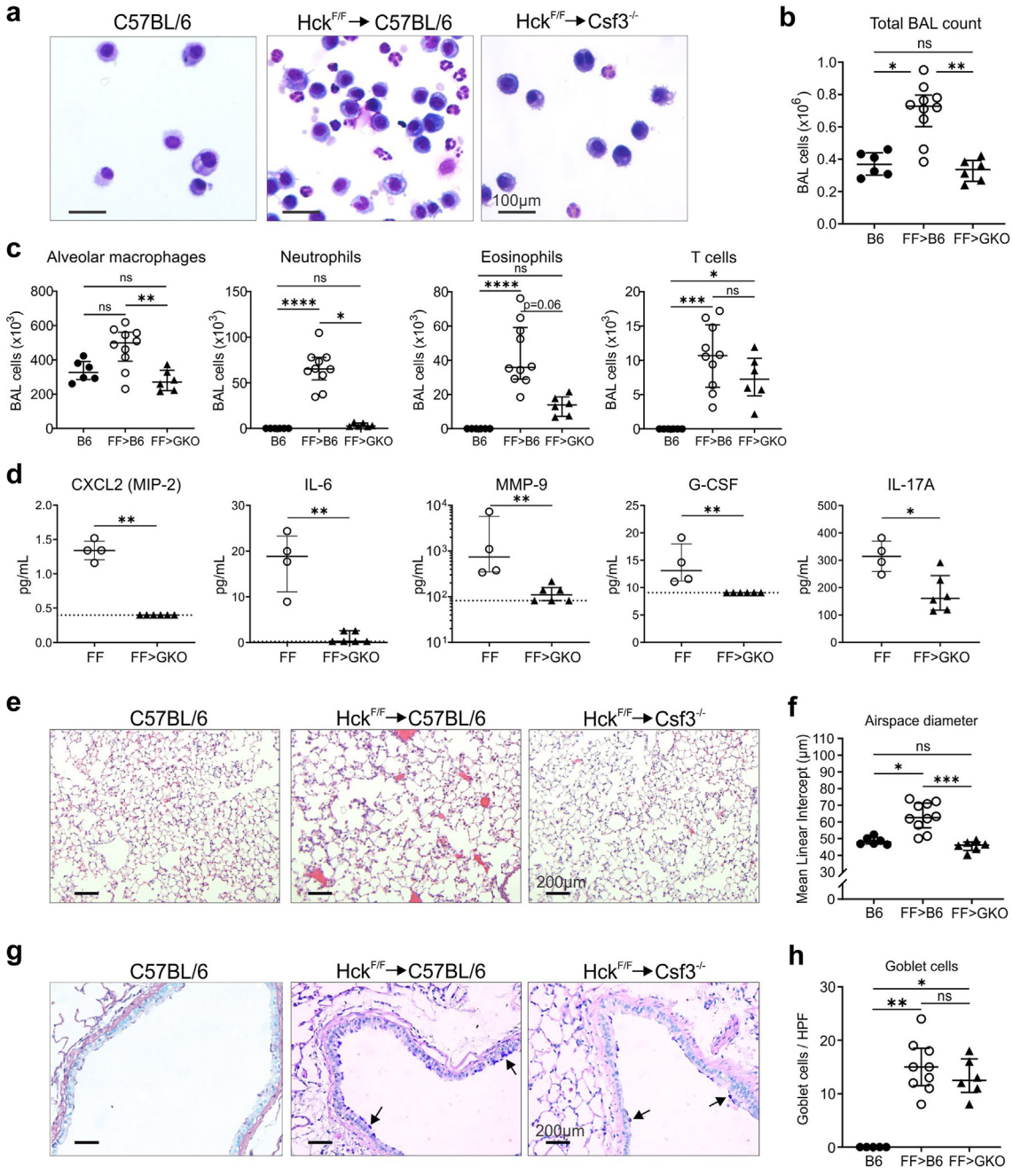

Fig. 4: **G-CSF produced by non-haematopoietic cells drives inflammation and emphysema but not goblet cell changes in Hck$^{F/F}$ mice.** BM chimeras were generated by transplanting Hck$^{F/F}$ BM into C57BL/6 or *Csf3*$^{-/-}$ mice (FF > B6 n = 10 and FF > GKO n = 6 respectively) and were analysed at 12 weeks post-transplant alongside C57BL/6 (B6, n = 6) mice as controls. (**a**) Morphological analysis of BAL cells, scale bars represent 100 µm; (**b**) BAL cell counts; and, (**c**) flow cytometric quantitation of immune cells in BAL. (**d**) Protein levels in BAL fluid of the FF > GKO chimeras (n = 6) alongside 20-wk-old Hck$^{F/F}$ mice (FF, n = 4) by multiplex assay, and IL-17A protein by ELISA. (**e**) Representative images of H&E-stained sections of the lung parenchyma, scale bars represent 200 µm; and, (**f**) corresponding quantitation of alveolar airspace size. (**g**) Representative images of the large airways of AB/PAS-stained lung cross-sections depicting mucus-producing goblet cells (arrows), scale bars represent 200 µm; and, (**h**) corresponding quantitation of goblet cell numbers. Data presented as median ± IQR. ns, not significant; **P* < 0.05, ***P* < 0.01, ****P* < 0.001, *****P* < 0.0001 (Kruskal–Wallis test with Dunn's post-test for b, c, f and h, and Mann–Whitney U test for d).

high power field compared to control (Fig. 4h, $P < 0.05$, Kruskal–Wallis test with Dunn's post-test). Overall, this indicates that non-haematopoietic cell-derived G-CSF is essential for the development of lung inflammation and emphysema but not goblet cell changes in $Hck^{F/F}$ mice. This also suggests that the haematopoietic compartment of $Hck^{F/F}$ mice is not the source of G-CSF, and instead is likely produced by lung stroma.

$Hck^{F/F}$ mice exhibit an expansion of activated T cells in BAL where HCK is expressed in γδ T cells but not conventional T cells

To further dissect the pulmonary inflammation in $Hck^{F/F}$ mice, the lymphocyte compartment of the BAL was examined. Alongside an expansion of myeloid cells in BAL (Fig. 2d, $P < 0.01$, Mann–Whitney U test), the inflammation included B cells ($P < 0.0001$), CD4+ T cells ($P < 0.001$), CD8+ T cells ($P < 0.0001$), NK cells ($P < 0.01$), and γδ T cells ($P < 0.0001$) (Fig. 5a, Mann–Whitney U test), with γδ T cells being defined as $CD3^+$ with a γδ T cell receptor (TCR). Further examination of BAL T cells revealed that γδ T cells were significantly activated in $Hck^{F/F}$ mice, as indicated by an increased number of $CD44^+CD62L^-$ effector memory (EM) T cells relative to naïve T cells (Fig. 5b, $P < 0.05$, Kruskal–Wallis test with Dunn's post-test). Thus, constitutive activation of HCK in mice results in not only activation of myeloid cells,[15] but also innate and adaptive lymphocytes, which suggests a broader role for HCK, and a possible role in T cell function.

HCK is expressed in myeloid cells and to a lesser extent in B lymphocytes but not T cells,[44,45] so finding increased numbers of conventional and unconventional T cells in the inflamed lung of $Hck^{F/F}$ mice prompted an in-depth examination of *Hck* expression in the T cell compartment. Quantitative PCR (qPCR) revealed that *Hck* was poorly detected in FACS-sorted conventional $CD4^+$ or $CD8^+$ T cells from C57BL/6 mouse spleen but was expressed in γδ T cells; however, at a lower level compared to mouse splenic B cells (Fig. 5c).

γδ T cell development is unaltered in $Hck^{F/F}$ mice

To determine if the expansion of γδ T cells in the lungs of $Hck^{F/F}$ mice correlated with altered T cell development, thymuses from 4-wk-old mice were examined by flow cytometry (Supplementary Figure S6a). No differences in numbers of double-negative (DN), double-positive, CD4+ or CD8+ thymocytes were observed in 4-wk-old $Hck^{F/F}$ mice compared to control

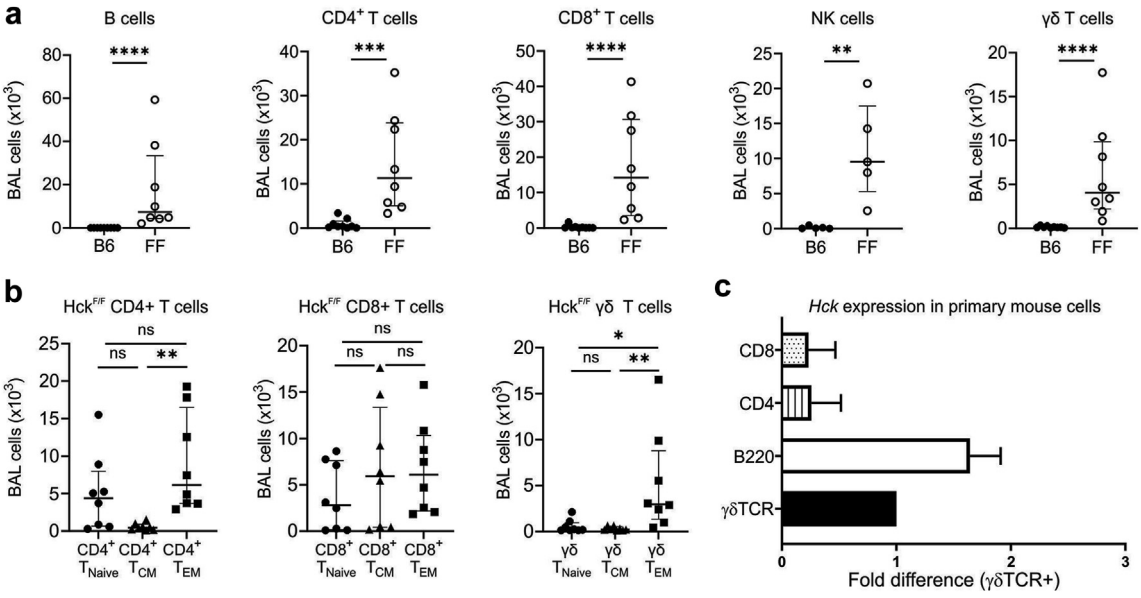

***Fig. 5:* γδ T cells are abundant in the BAL of $Hck^{F/F}$ mice and have an effector-memory phenotype.** (**a**) Flow cytometric quantification of the indicated lymphoid cells in BAL from 12-wk-old C57BL/6 (B6) and $Hck^{F/F}$ (FF) mice, n = 9 B6 and 8 FF mice per group from 2 experiments, except for NK cell analyses, where n = 5 per group from one experiment. (**b**) Numbers of $CD44^-CD62L^+$ naïve ($T_{naïve}$), $CD44^+CD62L^+$ central memory (T_{CM}) and $CD44^+CD62L^-$ effector memory (T_{EM}) $CD4^+$, $CD8^+$ and γδ T cells in the BAL of $Hck^{F/F}$ mice through CD62L vs CD44 gating, n = 8 mice/group from 2 independent experiments. Data presented as median ± IQR, ns = not significant; $^*P < 0.05$; $^{**}P < 0.01$; $^{***}P < 0.001$; $^{****}P < 0.0001$ (Mann–Whitney U test for a and Kruskal–Wallis test with Dunn's post-test for b). (**c**) Gene expression by qPCR of *Hck* in sorted CD8+ T cells, CD4+ T cells, B220+ B cells and γδTCR + T cells from C57BL/6 mouse spleen. Fold change was calculated relative to *Rn18s*. Three independent experiments were conducted and the data in each was normalised by expressing the fold difference relative to mouse γδ T cells; pooled data presented as mean ± SEM.

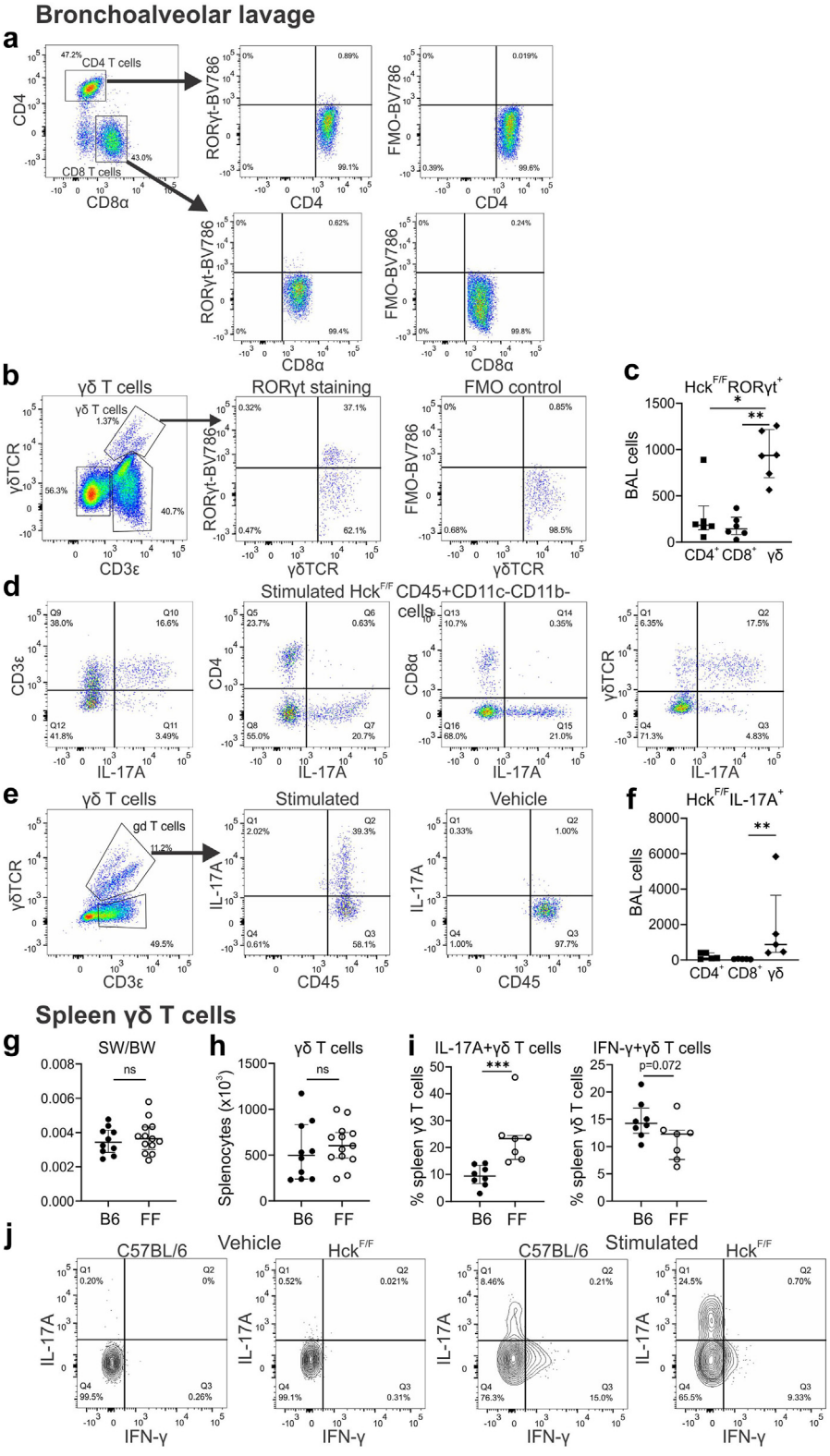

***Fig. 6:* γδ T cells in BAL of Hck$^{F/F}$ mice are skewed towards IL-17A production**. (**a**) Representative pseudocolour plots of RORγt staining of CD4$^+$ and CD8$^+$ T cells in BAL from Hck$^{F/F}$ mice, with FMO control. (**b**) Representative pseudocolour plots of RORγt staining of γδ T cells in BAL

(Supplementary Figure S6b, $P > 0.1$, Mann–Whitney U test). Furthermore, there were no differences in numbers of DN1-4, DN3a-c or DN4a-b thymocytes ($P > 0.1$, Mann–Whitney U test); however, there was a small but statistically significant increase in number of DN4c thymocytes in $Hck^{F/F}$ mice (Supplementary Figure S6c, $P = 0.0435$, Mann–Whitney U test). Numbers of γδTCR-expressing DN1-4 thymocytes were not different between C57BL/6 and $Hck^{F/F}$ mice (Supplementary Figure S6d, $P > 0.1$, Mann–Whitney U test), and there were no differences in γδTCR-expressing DN3a-c and DN4a-c thymocytes (Hsu AT, unpublished). As γδ T cells emerge from the DN stage, this indicates that HCK is unlikely to be involved in γδ T cell development. Although $CD3^{low}$ and $CD3^{high}$ γδ T cells were clearly evident in BAL (Supplementary Figure S1) and lung tissue samples (Supplementary Figure S2), in the thymus, $CD3^{low}$ and $CD3^{high}$ cells could not be distinguished as there was only one distinct $CD3^+$ population (Supplementary Figure S6a).

γδ T cells are a major source of IL-17A in $Hck^{F/F}$ lungs

Since IL-17A mediates neutrophilic inflammation,[40] is upstream of G-CSF,[40] and was present in the lungs of $Csf3^{-/-}$ mice reconstituted with $Hck^{F/F}$ BM (Fig. 4d), the cellular source of IL-17A was assessed. Staining for the transcription factor RORγt as a marker for IL-17A-producing cells[46] showed that conventional $CD4^+$ and $CD8^+$ T cells were largely $ROR\gamma t^-$ (Fig. 6a) while a notable percentage of γδ T cells in $Hck^{F/F}$ BAL were $ROR\gamma t^+$ (~37%) (Fig. 6b). Quantification of cell numbers revealed significantly more $ROR\gamma t^+$ γδ T cells (γδT17 cells) than $ROR\gamma t^+$ conventional T cells in $Hck^{F/F}$ BAL (Fig. 6c, $P < 0.01$, Kruskal–Wallis test). *Ex-vivo* stimulation of $Hck^{F/F}$ BAL cells with PMA and ionomycin showed that the majority of IL-17A was produced by γδ T cells, rather than $CD4^+$ and $CD8^+$ T cells (Fig. 6d and e), which was confirmed by quantification (Fig. 6f, $P < 0.001$, Kruskal–Wallis test). Additionally, dexamethasone treatment revealed that the γδ T cells in the BAL of $Hck^{F/F}$ mice were steroid-insensitive, with numbers unchanged (Supplementary Figure S7, $P = 0.7302$, Mann–Whitney U test). This suggests that γδ T cells, via IL-17A production, are drivers of lung disease in $Hck^{F/F}$ mice.

Splenic γδ T cells in $Hck^{F/F}$ mice are skewed towards IL-17A production

As γδT17 cells were expanded in BAL and implicated in the lung disease of $Hck^{F/F}$ mice, their responsiveness was assessed. Spleen was used as a source of γδ T cells (Supplementary Figure S8a), since they were not present in the BAL of C57BL/6 mice (Fig. 5a). Studies firstly showed that $Hck^{F/F}$ spleen was not obviously inflamed (Fig. 6g, $P = 0.6482$, Mann–Whitney U test) (Supplementary Figure S8b, c), there were no differences in the numbers of γδ T cells in the spleen of $Hck^{F/F}$ mice compared to C57BL/6 controls (Fig. 6h, $P = 0.3758$, Mann–Whitney U test), and numbers of splenic naïve ($P = 0.6049$), central memory ($P = 0.2839$) and effector memory ($P = 0.4100$) γδ T cells were similar (Supplementary Figure S8d, Mann–Whitney U test). In response to PMA and ionomycin stimulation, splenic γδ T cells from both C57BL/6 and $Hck^{F/F}$ mice were induced to produce either IL-17A or IFN-γ, but interestingly, $Hck^{F/F}$ mice displayed a higher percentage of γδ T cells producing IL-17A compared to control mice ($P < 0.001$, Mann–Whitney U test, Fig. 6i and j). This suggests that constitutive activation of HCK signalling in γδ T cells skews their responsiveness towards IL-17A production.

The Vγ6Vδ1 subset is increased in the lungs of $Hck^{F/F}$ mice

The TCR usage of γδ T cells correlates with their localisation and cytokine production.[47] To examine the TCR usage of the pulmonary γδ T cells in $Hck^{F/F}$ mice, $CD3^{high}$ and $CD3^{low}$ γδ T cells were sorted as single cells from digested lung tissue (Supplementary Figure S2) and spleen (Supplementary Figure S8a) of C57BL/6 and $Hck^{F/F}$ mice, and their TCR usage determined by single cell sequencing of the γδ TCR (Table 1, Supplementary Table S4). The $CD3^{high}$ population, present in C57BL/6 mice and enriched in the lungs of $Hck^{F/F}$ mice, were exclusively the invariant TRGV6-TRDV4/Vγ6Vδ1$^+$ subset (Table 1). In contrast, the $CD3^{low}$ γδ T cells in the lung had several invariant TCRs; however, Vγ6Vδ1$^+$ were more frequent in $Hck^{F/F}$ mice (70.5%) compared with C57BL/6 mice (31.25%) (Table 1). The remaining lung γδ T cell $CD3^{low}$ subsets were all TRGV4/Vγ4$^+$ expressing cells, with either TRDV2-2/Vδ4$^+$ or TRDV5/Vδ5$^+$ chains (Table 1).[48] Although no Vγ6Vδ1$^+$ cells were

from $Hck^{F/F}$ mice, with FMO control. (**c**) Quantification of RORγt-expressing cells in BAL of 4-wk-old $Hck^{F/F}$ mice, n = 6/group. (**d**) Representative pseudocolour plots depicting IL-17A staining of BAL from $Hck^{F/F}$ mice, stimulated for 4 h with PMA/ionomycin. $CD45^+CD11c^-CD11b^-$ cells were gated and assessed for $CD3^+$, $CD4^+$, $CD8^+$ and $\gamma\delta TCR^+$ cells. (**e**) Representative pseudocolour plots depicting IL-17A staining of γδ T cells in BAL from $Hck^{F/F}$ mice, stimulated with PMA/ionomycin, or vehicle. (**f**) Quantification of IL-17A-expressing cells in stimulated BAL from 6-wk-old $Hck^{F/F}$ mice, n = 5 mice/group. (**g**) Spleen weight (SW) as a proportion of body weight (BW) and (**h**) quantification of γδ T cells in the spleen of 12-wk-old mice by flow cytometry, (n = 10 B6 and 13 FF mice). (**i**) Proportion of IL-17A$^+$ and IFN-γ$^+$ γδ T cells in spleen after 4 h stimulation with PMA/ionomycin (n = 8 B6 and 7 FF). (**j**) Representative flow cytometry contour plots of IL-17A and IFN-γ staining of PMA/ionomycin stimulated splenic γδ T cells, with vehicle stimulated splenic γδ T cells shown as control. Data presented as median ± IQR. n = not significant; *$P < 0.05$, **$P < 0.01$, ***$P < 0.001$ (Mann–Whitney U test for g–i, and Kruskal–Wallis test with Dunn's post-test for c and f).

CD3	TRDV	CDR3δ	TRDJ	TRGV	CDR3γ	TRGJ	Frequency
C57BL/6 lung							
High	4	CGSDIGGSSWDTRQMFF	2	6	CACWDSSGFHKVF	1	21/21
Low	2–2	CALMEIWLPYRRDTNKLVF	1	–			1/16
	2–2	CALMERGIRATDKLVF	1	–			1/16
	4	CGSDIGGIRATDKLVF	1	6	CACWDSSGFHKVF	1	5/16
	5	CASGYIGGMSTDKLVF	1	4	CSYGLYSSGFHKVF	1	1/16
	5	CASGYIGGIRATDKVVF	1	–			5/16
	–			4	CSYGLYSSGFHKVF	1	3/16
HckF/F lung							
High	4	CGSDIGGSSWDTRQMFF	2	6	CACWDSSGFHKVF	1	23/23
Low	4	CGSDIGGSSWDTRQMFF	2	6	CACWDSSGFHKVF	1	12/17
	5	CASGSGGIRATDKLVF	1	4	CSYGYSSGFHKVF	1	1/17
	5	CASGIGGIRADKLVF	1	–			1/17
	5	CASGYIGGIRADKLVF	1	–			1/17
	5	CASGYIGGIRATDKLVF	1	–			1/17
	–			4	CSYGFYSSGFHKVF	1	1/17

[a]TRDV, TCR δ variable segment; CDR3δ, TCR δ complementarity-determining region 3; TRDJ, TCR δ junction segment; TRGV, TCR γ variable segment; CDR3γ, TCR γ complementarity-determining region 3; TRGJ, TCR γ junction segment. Sequences in red represent the invariant TRGV6-TRDV4/Vγ6Vδ1 TCR; '–' represents not determined.

Table 1: **TCR usage of $CD3^{high}$ and $CD3^{low}$ γδ T cells in lung of C57BL/6 and $Hck^{F/F}$ mice.[a]**

detected in the spleen of C57BL/6 mice, they were present, albeit infrequently, in $Hck^{F/F}$ spleen in the $CD3^{high}$ population, while the spleen of both C57BL/6 and $Hck^{F/F}$ mice had mainly TRGV1/Vγ1$^+$, TRGV2/Vγ2$^+$ and TRGV4/Vγ4$^+$ subsets (Supplementary Table S4). Thus, the Vγ6Vδ1$^+$ subset is preferentially expanded in the lungs of $Hck^{F/F}$ mice. Vγ6Vδ1$^+$ cells were also detected at a lower frequency in the spleen of $Hck^{F/F}$ mice but not C57BL/6 mice.

Deficiency of γδ T cells does not alter IL-17A production or lung disease in $Hck^{F/F}$ mice

To determine if γδT17 cells were the primary initiators of lung disease in $Hck^{F/F}$ mice, double mutant $Hck^{F/F}Tcrd^{-/-}$ mice were generated, with flow cytometry confirming that γδ T cells were absent (Supplementary Figure S9a). Upon phenotyping of $Hck^{F/F}Tcrd^{-/-}$ mice, it was apparent that the absence of γδT cells did not attenuate lung disease. Goblet cells were clearly present in the conducting airways of 4-wk-old $Hck^{F/F}Tcrd^{-/-}$ mice (Fig. 7a), with numbers increased similarly to $Hck^{F/F}$ mice (Fig. 7b, $P < 0.05$, Kruskal–Wallis test with Dunn's post-test), and elevated *Muc5ac* and *Muc5b* gene expression was evident in lung tissue (Fig. 7c, $P < 0.05$, Kruskal–Wallis test with Dunn's post-test). The lungs of 12-wk-old $Hck^{F/F}Tcrd^{-/-}$ mice were obviously inflamed and emphysematous (Fig. 7d), and morphometry showed that the airspaces of $Hck^{F/F}Tcrd^{-/-}$ mice were enlarged like those in $Hck^{F/F}$ mice (Fig. 7e, $P < 0.001$, Kruskal–Wallis test with Dunn's post-test). Moreover, deletion of γδ T cells in $Hck^{F/F}$ mice did not reduce lung gene expression of *Csf3* or *Il17a* (Fig. 7f, $P < 0.05$, Mann–Whitney U test). Lastly, $Hck^{F/F}Tcrd^{-/-}$ mice exhibited lung inflammation with inflammatory cells in BAL (Fig. 7g), and BAL cell counts were elevated similarly to $Hck^{F/F}$ mice (Fig. 7h, $P < 0.0001$ for 4-wk-old mice and $P < 0.001$ for 12-wk-old mice, Kruskal–Wallis test with Dunn's post-test). Unabated inflammation was also observed in 4-wk-old $Hck^{F/F}Tcrd^{-/-}$ mice, with increases in immune cells in BAL (Supplementary Figure S9b, $P < 0.001$ for neutrophils, $P < 0.01$ for monocytes, CD4 T cells and CD8 T cells, Kruskal–Wallis test with Dunn's post-test) and myeloid cells in lung tissue (Supplementary Figure S9c, $P < 0.0001$ for alveolar macrophages, $P < 0.01$ for neutrophils and eosinophils, Kruskal–Wallis test with Dunn's post-test). Thus, deletion of γδ T cells in $Hck^{F/F}$ mice did not alter their lung disease and did not induce the loss of IL-17A, suggesting another cellular source of IL-17A in these γδ T cell-deficient mice.

Lung MAIT17 cells are markedly expanded in $Hck^{F/F}Tcrd^{-/-}$ mice

Since $Hck^{F/F}$ mice lacking γδ T cells retained IL-17A expression, alternative IL-17A-producing cells were considered, including group 3 innate lymphoid cells (ILC), MAIT cells and NKT cells. Staining for RORγt$^+$ cells in BAL revealed an absence of RORγt$^+$ CD4$^+$ and CD8$^+$ T cells, indicating that these subsets did not contribute to IL-17A production in $Hck^{F/F}Tcrd^{-/-}$ mice (Supplementary Figure S9d). Flow cytometry of cells from digested lung tissue showed that lineage$^-$ CD127$^+$ ILC1, ILC2 and ILC3 cells were similarly present in the lungs of all mice (Fig. 8a). However, there was a marked increase in CD3$^+$ cells expressing RORγt in $Hck^{F/F}Tcrd^{-/-}$ mice, indicating that a subset of IL-17A-producing T cells are engendered in the absence of γδ T cells (Fig. 8a, $P < 0.01$, Kruskal–Wallis test with Dunn's post-test). Staining lung tissue digests using CD1d-α-GalCer tetramers showed no differences in

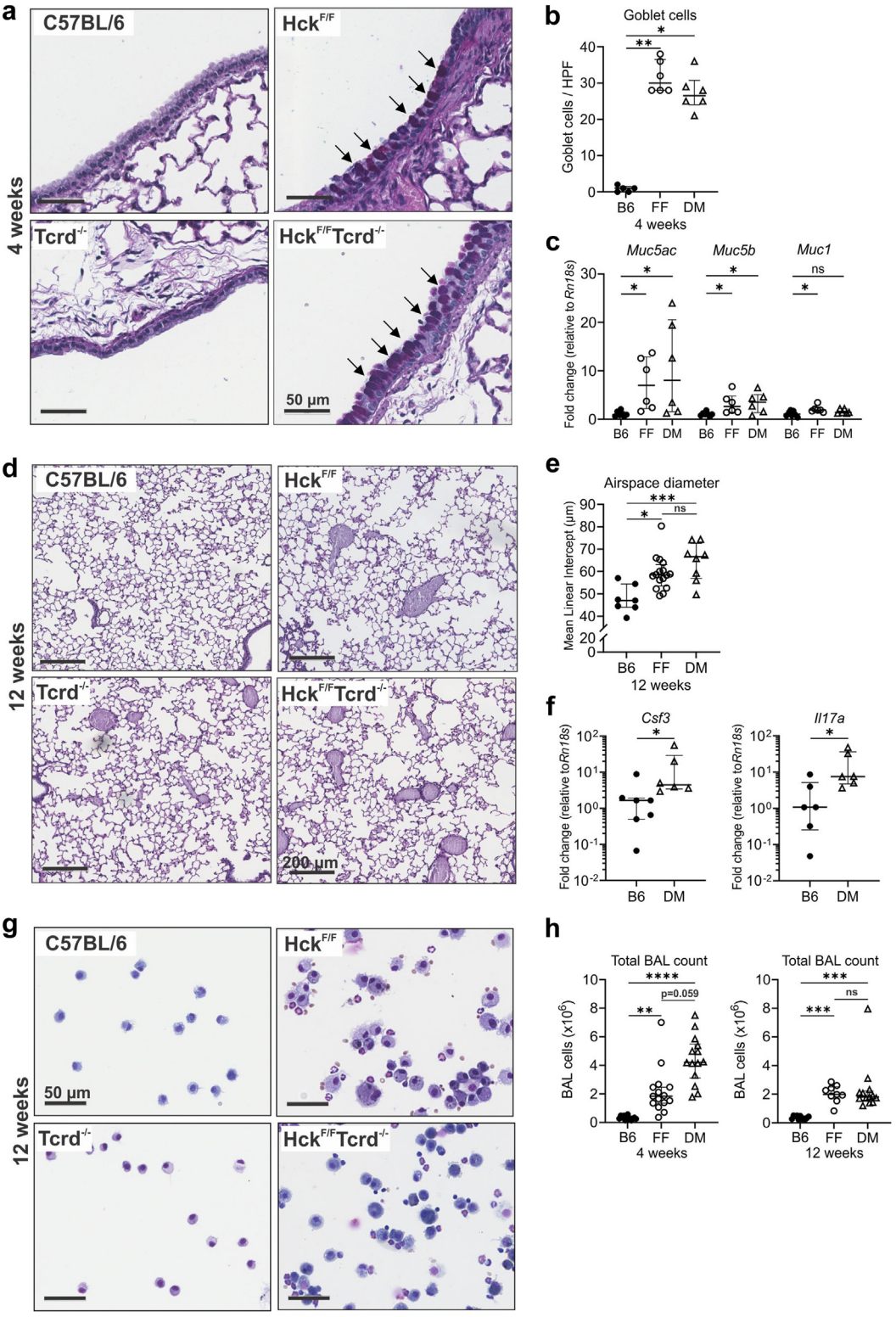

***Fig. 7*: Deletion of γδ T cells in Hck$^{F/F}$ mice does not reduce lung disease or inflammation**. (**a**) Representative images of AB/PAS-stained lung cross-sections from 4-wk-old C57BL/6 (B6), Hck$^{F/F}$ (FF), Tcrd$^{-/-}$ and Hck$^{F/F}$Tcrd$^{-/-}$ (DM) mice depicting large airways and mucus-producing goblet cells (arrows), scale bars represent 50 µm; and, (**b**) corresponding quantitation of goblet cells (n = 5 B6, 6 FF and 6 DM). (**c**) Gene

numbers of NKT cells (Fig. 8b and c). However, staining with MR1-5-OP-RU tetramers revealed that MAIT cells were markedly expanded in the lungs of $Hck^{F/F}Tcrd^{-/-}$ mice ($P < 0.0001$, Kruskal–Wallis test with Dunn's post-test), and to a lesser extent in $Tcrd^{-/-}$ mice ($P < 0.05$, Kruskal–Wallis test with Dunn's post-test), and were notably lower in frequency and number in the lung tissue of C57BL/6 and $Hck^{F/F}$ mice (Fig. 8b and d). MAIT cells in $Hck^{F/F}Tcrd^{-/-}$ BAL were predominantly RORγt$^+$, indicative of their capacity to produce IL-17A (Fig. 8e), and a higher number of RORγt$^+$ MAIT (MAIT17) cells were present in $Hck^{F/F}Tcrd^{-/-}$ BAL relative to $Hck^{F/F}$ BAL (Fig. 8f, $P < 0.01$, Mann–Whitney U test). Thus, deficiency of γδ T cells induces a niche-filling effect, leading to the compensatory expansion of RORγt$^+$ MAIT17 cells in the lungs of $Hck^{F/F}Tcrd^{-/-}$ mice.

IL-17A drives lung disease in $Hck^{F/F}$ mice

The role of IL-17A in lung disease was next investigated by generating $Hck^{F/F}Il17a^{-/-}$ mice. Lung histopathology showed that goblet cell numbers were attenuated in $Hck^{F/F}Il17a^{-/-}$ mice (Fig. 9a), with goblet cells infrequently observed and numbers comparable to control mice (Fig. 9b, $P > 0.9999$, Kruskal–Wallis test with Dunn's post-test). Age-dependent emphysema (Fig. 9c) was abrogated in $Hck^{F/F}Il17a^{-/-}$ mice (Fig. 9d, $P = 0.7043$, Kruskal–Wallis test with Dunn's post-test) and lung inflammation was markedly reduced in $Hck^{F/F}Il17a^{-/-}$ mice (Fig. 9e, $P = 0.1256$, Kruskal–Wallis test with Dunn's post-test), with numbers of neutrophils, eosinophils and γδ T cells in BAL not significantly different compared to C57BL/6 control mice (Fig. 9f, $P > 0.1$, Kruskal–Wallis test with Dunn's post-test), indicating that IL-17A underlies the development of both. Collectively, these data establish that dysregulated IL-17A production underlies lung disease development in $Hck^{F/F}$ mice, driving both mucus overproduction and emphysema, and implicates HCK as a regulator of IL-17A-driven lung pathologies. Furthermore, these studies suggest that γδ T cells and MAIT cells are a key source of IL-17 that may precipitate this disease.

Discussion

In this study, we have probed fundamental mechanisms of obstructive lung disease, placing HCK at the apex of a nexus between an IL-17A/G-CSF/granulocyte axis; a reciprocal niche dynamic between γδ T cells and MAIT cells; and the interplay of the lung stromal and myeloid cell compartments in inflammation, goblet cell hyperplasia/metaplasia, and tissue destruction (Fig. 10). As we have investigated the unfolding of disease, our study provides molecular ontological insights into early disease susceptibility determinants and suggests that targeting HCK may ameliorate COPD pathogenesis and its progression by 'upstream' regulation of multiple effector pathways, both in established COPD and the emerging category of pre-COPD.

Primary mutations in HCK are infrequent in COPD but HCK is a nodal convergence point in multiple pathways implicated in its pathogenesis. We propose that in chronic lung disease, HCK, via IL-17A, drives G-CSF, which supports the development of BM myeloid cells, stimulates their activation, and promotes their survival in lung tissue where they sustain inflammation, leading to lung tissue destruction. G-CSF levels are elevated in smokers and smokers with COPD, and genetic variation in G-CSF is associated with lung function impairment in smokers.[49] We have recently demonstrated that G-CSF is a critical mediator of COPD and its complex comorbidities in an independent experimental model[19]; however, it is clear that G-CSF is implicated in multiple lung diseases including acute respiratory distress syndrome,[50] idiopathic pulmonary fibrosis,[51] acute chest syndrome,[52] severe asthma,[53] and bronchopulmonary dysplasia.[54]

Notwithstanding that G-CSF promotes neutrophil activity,[18] and neutrophil elastase is a potent stimulator of mucus production and secretion,[3–6] BM chimeras revealed that G-CSF deficiency in the lung stromal compartment did not ablate increased goblet cell numbers, while deletion of IL-17A, the upstream inducer of G-CSF,[40] resulted in a loss of all lung disease traits. IL-17A is a potent driver of mucus metaplasia,[41,55,56] and blocking IL-17A reduces disease in multiple COPD models.[57,58] To date, small and unstratified trials targeting IL-17A in COPD have not been successful.[59] Our data suggests that targeting IL-17A and/or cellular sources of IL-17A could be reconsidered for COPD treatment if patients exhibited an "HCK endotype" that might include an IL-17A inflammatory signature, G-CSF upregulation, and mucus plugging. Moreover, this approach may also be successful in early or pre-COPD with this underlying signature. In $Hck^{F/F}$ mice, lung inflammation—including eosinophilia—was

expression of *Muc5ac*, *Muc5b* and *Muc1* in whole lung tissue of the indicated groups of 4-wk-old mice (n = 7 B6, 6 FF and 6 DM). (**d**) Representative images of AB/PAS-stained lung cross-sections from the indicated groups of 12-wk-old mice, scale bars represent 200 μm; and, (**e**) corresponding quantitation of alveolar airspace size (n = 7 B6, 16 FF and 8 DM). (**f**) Gene expression of *Il17a* and *Csf3* in whole lung tissue of the indicated groups of 4-wk-old mice (n = 7 B6 and 6 DM). (**g**) Morphological analysis of BAL cells from the indicated 12-wk-old mice; scale bars represent 50 μm. (**h**) BAL cell counts from the indicated groups of 4-wk-old mice (n = 13 B6, 15 FF and 14 DM) and 12-wk-old mice (n = 11 B6, 9 FF and 13 DM). Data presented as median ± IQR. ns, not significant; *$P < 0.05$, **$P < 0.01$, ***$P < 0.001$, ****$P < 0.0001$ (Kruskal–Wallis test with Dunn's post-test).

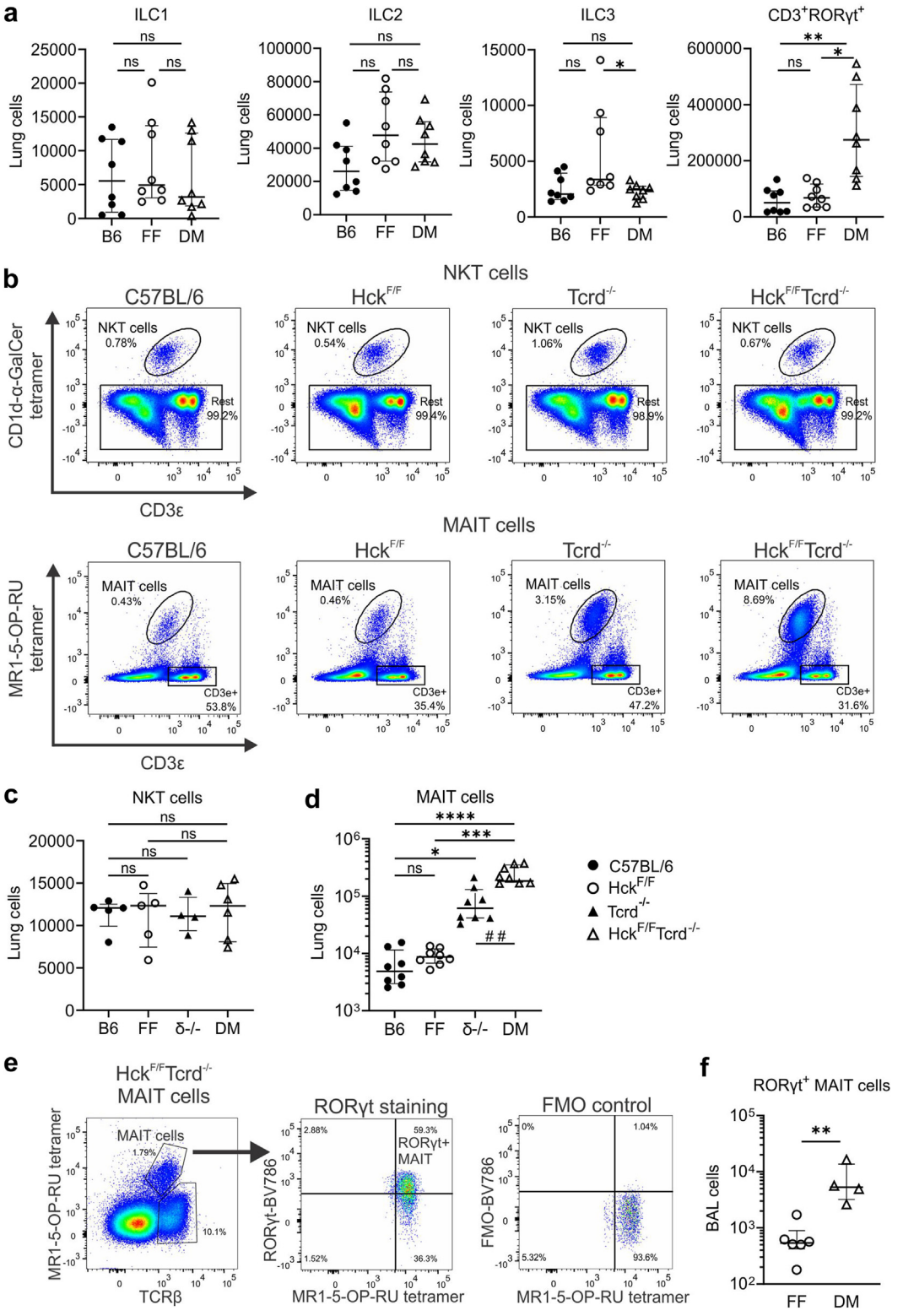

Fig. 8: **Deficiency of γδ T cells in Hck$^{F/F}$ mice results in expansion of pulmonary MAIT cells**. Quantification of (**a**) ILC1, ILC2, ILC3, and CD3^{+}RORγt^{+} cells in digested lung tissue of 12-wk-old C57BL/6 (B6), Hck$^{F/F}$ (FF) and Hck$^{F/F}$Tcrd$^{-/-}$ (DM) mice by flow cytometry, n = 8/per group. (**b**) Representative pseudocolour plots of lung tissue cells from the indicated groups of mice stained for NKT and MAIT cells. (**c**) Flow

glucocorticoid-insensitive, and this finding is supported by the poor steroid response of a patient with early-onset respiratory disease that harboured an activating mutation in *HCK*.[13] A very diverse range of steroid molecules are used by multiple routes (inhalation alone or in combination therapy, orally, parenteral injection) in the clinical management of COPD. Dexamethasone was used in our study because it is clinically relevant and has excellent systemic and lung bioavailability after intraperitoneal administration in mice. Interestingly, eosinophilic inflammation, which is found in about one-third of patients with COPD, is a biomarker of possible glucocorticoid responsiveness.[60] However, it is not the number of eosinophils, but rather their reduction after steroids that is the most informative biomarker, as many patients have steroid-refractory/insensitive eosinophilia. This reduced response to steroids is of considerable clinical interest and it is possible that our $Hck^{F/F}$ model may provide additional insights into underlying mechanisms in future studies.

Originally thought to be myeloid and B cell-specific[44,45]; we now formally show that *Hck* is also expressed in mouse γδ T cells but not conventional T cells. This finding is supported by published datasets from the Immunological Genome Project which reveal that *Hck* is expressed at low levels in splenic γδ T cells but not conventional αβ T cells in mice (Supplementary Figure S10).[61] We probed this and found that in $Hck^{F/F}$ mice, γδ T cells become pathogenic and contribute to lung disease. This is almost certainly via constitutive activation of HCK signalling, which likely heightens their responsiveness, alters their cytokine programming, and induces them to expand locally. Expansion of γδ T cells in the lungs of $Hck^{F/F}$ mice could be driven in response to specific signals that trigger the HCK signalling pathway, which is already primed for responsiveness by the gain-of-function mutation.[15] Furthermore, activated γδ T cells are known to produce chemokines,[47] which may also contribute to pulmonary inflammation in $Hck^{F/F}$ mice. It is well known that the specific type of TCR used by γδ T cells correlates both with their localisation and cytokine production. Vγ6Vδ1-expressing γδ T cells are commonly represented in the lung[47] and they predominantly produce IL-17A.[62] Furthermore, γδ T cells with high expression of CD3 are linked to IL-17A production.[48] The expanded population of pulmonary γδ T cells in $Hck^{F/F}$ mice were Vγ6Vδ1-expressing and $CD3^{bright}$, they expressed the transcription factor RORγt, indicative of their capacity to produce IL-17A, and moreover, upon *ex vivo* stimulation, they were skewed towards IL-17A production. Collectively, these features strongly suggest that they are γδT17 cells. Mouse lung γδT17 cells are increased by cigarette smoke-exposure, driving macrophage inflammation,[63] and furthermore, γδT17 cells contribute to elastase-induced emphysema in mice.[64] However, there is currently little evidence that γδ T cells themselves drive IL-17A production and disease in COPD. In fact, γδ T cells may be protective,[65] and γδ T cell numbers are reportedly reduced in patients with COPD.[66,67] Thus, other IL-17A-producing cells, such as conventional $CD4^+$ and $CD8^+$ T cells, which are abundant in the COPD lung,[68–70] and MAIT cells,[71] may play a greater role in disease progression in COPD.

Global deletion of γδ T cells in $Hck^{F/F}$ mice led to marked expansion of pulmonary MAIT17 cells. This finding is supported by recent reports of the compensatory increase of thymic and peripheral MAIT cells following deletion of either or both γδ T cells and NKT cells.[72,73] The pronounced increase of MAIT cells in $Hck^{F/F}Tcrd^{-/-}$ mice indicates this effect is compounded in a lung disease setting. HCK is also expressed in MAIT cells, particularly human blood MAIT cells (Supplementary Figure S10),[61] suggesting that HCK signalling may also be involved in MAIT cell activation, driving their expansion in the absence of γδ T cells in $Hck^{F/F}Tcrd^{-/-}$ mice to fill an immunological niche. Pulmonary MAIT17 cells, similar to $ROR\gamma t^+$ NKT17 cells and γδT17 cells, can respond to analogous stimuli to elicit IL-17A-mediated protection against respiratory infections.[74] In the absence of γδ T cells, MAIT cells likely respond and expand to similar environmental signals as γδ T cells through HCK signalling. The reason for this restrained response when γδ T cells are present is not clear, yet suggests a delicate balance of niche dynamics between these unconventional T cells in the lung. Our findings support an exquisite redundancy between distinct cellular sources of IL-17A, i.e. γδ T cells and MAIT cells, providing an important insight into how targeting one cell type may elicit a compensatory response from another.

Our study has strengths and limitations which should be stated. A strength is that our mouse genetic model shows an amplified and accelerated phenotype; however, this is also a translational caveat, also presenting a limitation. It will be of great interest, and essential, to now study clinical correlations and new HCK endotypes. Goblet cells, which are sparse in the

cytometric quantitation of NKT cells in lung tissue digests of 12-wk-old mice (n = 5 B6, 5 FF, 4 $Tcrd^{-/-}$ (δ−/−) and 6 DM), and (**d**) flow cytometric quantitation of MAIT cells in lung tissue digests of 12-wk-old mice, n = 8 mice/group. (**e**) Representative flow cytometry pseudocolour plots of BAL cells from $Hck^{F/F}Tcrd^{-/-}$ mice gated on MAIT cells and examined for RORγt staining, with FMO control. (**f**) Flow cytometric quantitation of $ROR\gamma t^+$ MAIT cells in BAL of $Hck^{F/F}$ mice (n = 6) and $Hck^{F/F}Tcrd^{-/-}$ mice (n = 4). Data presented as median ± IQR. ns, not significant; *$P < 0.05$, **$P < 0.01$, ***$P < 0.001$, ****$P < 0.0001$ (Kruskal–Wallis test with Dunn's post-test for a, c and d, and Mann–Whitney U test for f). In (d), ##$P < 0.01$ comparing $Tcrd^{-/-}$ (δ−/−) and $Hck^{F/F}Tcrd^{-/-}$ mice (Mann–Whitney U test).

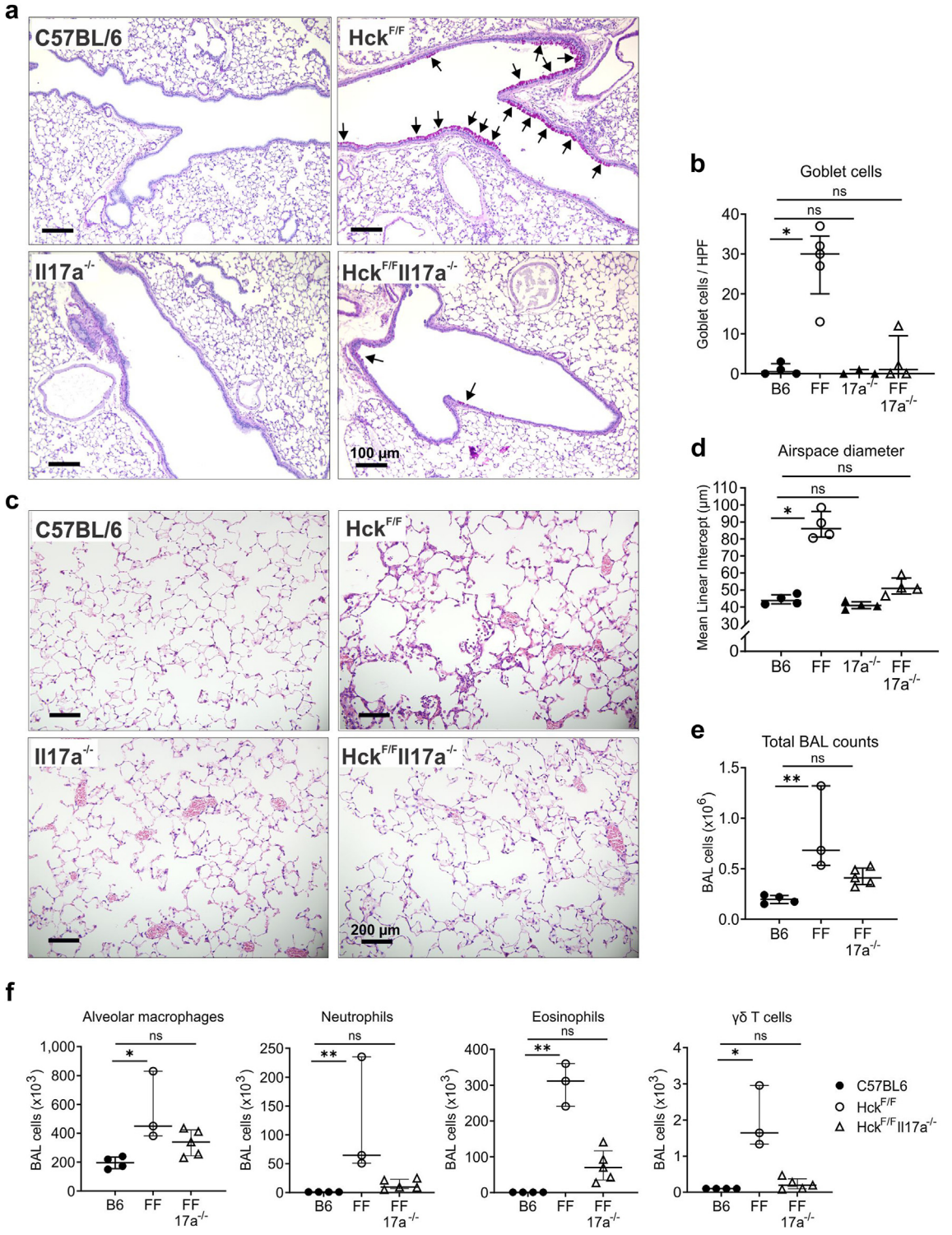

Fig. 9: **IL-17A drives lung inflammation, emphysema and goblet cell changes in Hck$^{F/F}$ mice**. (**a**) Representative AB/PAS-stained lung cross-sections from 6-wk-old C57BL/6 (B6), Hck$^{F/F}$ (FF) and Hck$^{F/F}$Il17a$^{-/-}$ (FF17a$^{-/-}$) mice depicting mucus-producing goblet cells in large airways (arrows), scale bars represent 100 µm; and, (**b**) quantification of goblet cells per high power field (HPF) in large airways (n = 4 B6, 5 FF, 3 Il17a$^{-/-}$, 4 FF17a$^{-/-}$). (**c**) Representative H&E-stained lung cross-sections of the indicated groups of 60-wk-old mice; scale bars represent

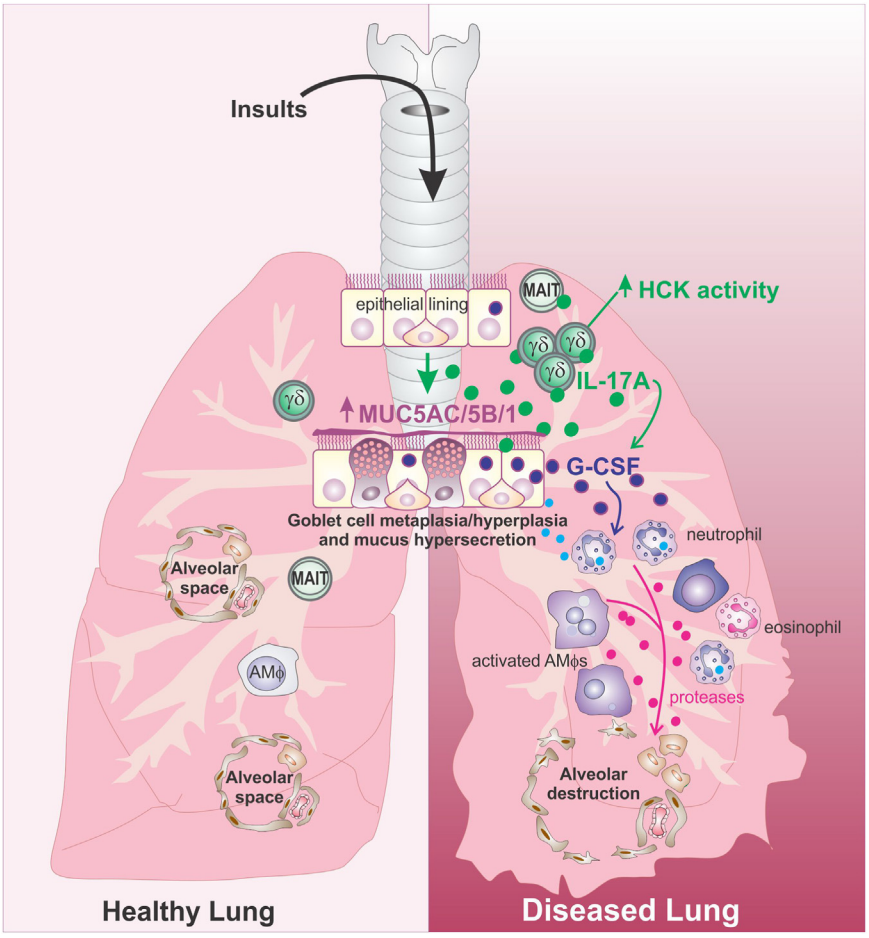

***Fig. 10*: IL-17A-producing unconventional T cells drive HCK-mediated lung disease**. γδ T cells and MAIT cells are present in the healthy lung, and together with alveolar macrophages (AMϕ) serve as a first line of defence. In obstructive airways disease, induced by various lung insults, HCK becomes chronically activated, driving an 'HCK/IL-17 disease endotype' where HCK-expressing γδ T cells induce goblet cell changes and mucus hypersecretion via IL-17A production, and promote destructive myeloid-rich inflammation via G-CSF.

large airways of mice,[75] can arise by both metaplasia and hyperplasia; however, whether the increase in goblet cell numbers in $Hck^{F/F}$ mice represents metaplasia or hyperplasia was not discerned in this study, which also represents a limitation. Another strength is that we have been able to use sophisticated bone marrow chimeras and knockout mice to discern disease mechanisms, uncovering the role of IL-17A-producing unconventional T cells. However, a limitation is that we do not yet know to what the unconventional T cells in our mutant mice are responding. Nonetheless, these mutants will be valuable models for the study of γδT17 cell and MAIT17 cell activation and function. In addition, it will now be important to treat $Hck^{F/F}$ mice with anti-IL-17 or small molecule RORγt inhibitors to demonstrate clinical applicability for pulmonary diseases with an HCK/IL-17 endotype in a precision medicine approach.

Further work examining γδ T cells at other mucosal sites in $Hck^{F/F}$ mice is now warranted, as well as testing of the pulmonary immune response of these mice to cigarette smoke and pathogens. It would also be interesting to examine the γδ T cell compartment of Hck-deficient mice[76] and assess their response to lung insults such as cigarette smoke. Nonetheless, our work identifies HCK as an important therapeutic target at the apex of an IL-17A/G-CSF/granulocyte and unconventional T cell pathogenic axis that offers improved insights into the fundamental pathobiology of COPD.

200 μm; and, (**d**) corresponding alveolar airspace size; n = 4 mice per group. (**e**) Total BAL cell counts in indicated groups of 6-wk-old mice, and (**f**) corresponding flow cytometric quantitation of BAL cell composition (n = 4 B6, 3 FF, 5 $FF17a^{-/-}$). Data presented as median ± IQR. ns, not significant; *$P < 0.05$, **$P < 0.01$ (Kruskal–Wallis with Dunn's post-test).

Given that HCK is highly 'druggable', we suggest that HCK inhibitors will emerge as a therapeutic strategy in COPD, pre-COPD, and by inference, their complex comorbidome.

Contributors

Conceptualisation: ME, GPA, MLH; Methodology: ATH, RJJO, ET, TAG, JGB, NAG, CX, HFK; Investigation: ATH, RJJO, ET, TAG, JGB, NAG; Visualisation: ATH; Resources: DIG, ME, MLH; Supervision: ET, TAG, DIG, ME, MLH; Writing—original draft: ATH, GPA, MLH; Writing—review and editing: ATH, RJJO, ET, TAG, NAG, CX, HFK, DIG, ME, GPA, MLH; Funding acquisition: ME, GPA, MLH. ATH, NAG, ME, and MLH verified the data reported in the manuscript. All authors read an approved the final version of the manuscript.

Data sharing statement

All data collected for the study that underpins the conclusions are presented in the main paper and the Supplementary Materials, and data can be shared by the corresponding author upon reasonable request.

Declaration of interests

ATH and TAG received funding to attend the Australian and New Zealand Society of Immunology conference in 2022 and 2023 respectively; GPA received funding from RAGE Biotechnology, acted as a consultant for RAGE Biotechnology, ENA Respiratory and Pieris Pharmaceuticals, received honoraria from AstraZeneca, GSK and Sanofi, support from Griffith University and Thoracic Society of Australia and New Zealand (TSANZ), participated on Data Safety Monitoring Boards for PACE and INHERIT studies, was a Board Member of TSANZ, and received stock options from ENA Respiratory; and, MLH received grant funding from Lupus Research Alliance and RAGE Biotechnology. The remaining authors declare that they have no competing interests.

Acknowledgements

The authors thank Maverick Lau, PhD, who contributed to the early studies in this project. The authors gratefully acknowledge the assistance of technicians from the Monash Animal Research Platform, the Monash Intensive Care Unit and the Precinct Animal Centre for animal breeding and husbandry, and the technical assistance and use of services within the Monash Histology Facility, Monash Micro Imaging and Alfred Research Alliance Flow Core. We are grateful to A/Prof Alexandra Corbett from The Peter Doherty Institute for Infection and Immunity and The University of Melbourne, Melbourne, Australia for providing reagents for the study. The $Hck^{F/F}$ mice are held under a Material Transfer Agreement with the Ludwig Institute for Cancer Research, New York, NY, USA and thus cannot be freely distributed without an agreement in place.

This work was supported by an Australian Government Research Training Program Stipend administered by Monash University and paid to ATH; a Victoria Cancer Agency Early Career Seed Grant (ECSG13041) paid to RJJO; National Health and Medical Research Council Australia (NHMRC) Project Grant (APP1025239) paid to RJJO; NHMRC Emerging Leadership Grant (2027058; 2024–2028) paid to NAG; Australian Research Council Discovery Early Career Research Award (210100705; 2021–2023) paid to NAG; Australian Government Research Training Program Stipend administered by Peter Doherty Institute for Infection and Immunity and paid to CX; Australian Research Council Discovery Early Career Researcher Award (DE220100830; 2023–2025) paid to HFK; NHMRC Investigator Grant (2008913; 2022–2026) paid to DIG; NHMRC Project Grants (APP1079257 and APP1081373) paid to ME; NHMRC Investigator Grant (APP1173814; 2020–2024) paid to ME; NHMRC Project Grants (APP1080274 and APP1147267) paid to GPA; NHMRC Project Grants (APP1080274 and APP1147267) paid to MLH; Monash University Salary Support paid to MLH.

Appendix A. Supplementary data

Supplementary data related to this article can be found at https://doi.org/10.1016/j.ebiom.2025.105707.

References

1 Boers E, Barrett M, Su JG, et al. Global burden of chronic obstructive pulmonary disease through 2050. *JAMA Netw Open*. 2023;6(12):e2346598.
2 Vestbo J, Prescott E, Lange P. Association of chronic mucus hypersecretion with FEV1 decline and chronic obstructive pulmonary disease morbidity. Copenhagen City Heart Study Group. *Am J Respir Crit Care Med*. 1996;153(5):1530–1535.
3 Takeyama K, Agustí C, Ueki I, Lausier J, Cardell LO, Nadel JA. Neutrophil-dependent goblet cell degranulation: role of membrane-bound elastase and adhesion molecules. *Am J Physiol*. 1998;275(2):L294–L302.
4 Fischer BM, Voynow JA. Neutrophil elastase induces MUC5AC gene expression in airway epithelium via a pathway involving reactive oxygen species. *Am J Respir Cell Mol Biol*. 2002;26(4):447–452.
5 Voynow JA, Fischer BM, Malarkey DE, et al. Neutrophil elastase induces mucus cell metaplasia in mouse lung. *Am J Physiol Lung Cell Mol Physiol*. 2004;287(6):L1293–L1302.
6 Shao MX, Nadel JA. Neutrophil elastase induces MUC5AC mucin production in human airway epithelial cells via a cascade involving protein kinase C, reactive oxygen species, and TNF-alpha-converting enzyme. *J Immunol*. 2005;175(6):4009–4016.
7 Hiemstra PS, van Wetering S, Stolk J. Neutrophil serine proteinases and defensins in chronic obstructive pulmonary disease: effects on pulmonary epithelium. *Eur Res J*. 1998;12(5):1200–1208.
8 Quint JK, Ariel A, Barnes PJ. Rational use of inhaled corticosteroids for the treatment of COPD. *NPJ Prim Care Respir Med*. 2023;33(1):27.
9 Poh AR, Love CG, Masson F, et al. Inhibition of hematopoietic cell kinase activity suppresses myeloid cell-mediated colon cancer progression. *Cancer Cell*. 2017;31(4):563–575.e5.
10 Zhang X, Mahmudi-Azer S, Connett JE, et al. Association of Hck genetic polymorphisms with gene expression and COPD. *Hum Genet*. 2007;120(5):681–690.
11 Yanagisawa S, Sugiura H, Yokoyama T, et al. The possible role of hematopoietic cell kinase in the pathophysiology of COPD. *Chest*. 2009;135(1):94–101.
12 Liu L, Huang N, Chen L, Wang XZ, Yang XD. Hematopoietic cell kinase gene polymorphisms and the risk of chronic obstructive pulmonary disease in a Chinese population. *Exp Lung Res*. 2012;38(1):37–42.
13 Kanderova V, Svobodova T, Borna S, et al. Early-onset pulmonary and cutaneous vasculitis driven by constitutively active SRC-family kinase HCK. *Allergy Clin Immunol*. 2022;149(4):1464–1472.e3.
14 Poh AR, O'Donoghue RJ, Ernst M. Hematopoietic cell kinase (HCK) as a therapeutic target in immune and cancer cells. *Oncotarget*. 2015;6(18):15752–15771.
15 Ernst M, Inglese M, Scholz GM, et al. Constitutive activation of the SRC family kinase Hck results in spontaneous pulmonary inflammation and an enhanced innate immune response. *J Exp Med*. 2002;196(5):589–604.
16 Duan M, Steinfort DP, Smallwood D, et al. CD11b immunophenotyping identifies inflammatory profiles in the mouse and human lungs. *Mucosal Immunol*. 2016;9(2):550–563.
17 Le Rouzic O, Pichavant M, Frealle E, Guillon A, Si-Tahar M, Gosset P. Th17 cytokines: novel potential therapeutic targets for COPD pathogenesis and exacerbations. *Eur Respir J*. 2017;50(4):1602434.
18 Panopoulos AD, Watowich SS. Granulocyte colony-stimulating factor: molecular mechanisms of action during steady state and 'emergency' hematopoiesis. *Cytokine*. 2008;42(3):277–288.
19 Tsantikos E, Lau M, Castelino CM, et al. Granulocyte-CSF links destructive inflammation and comorbidities in obstructive lung disease. *J Clin Invest*. 2018;128(1):2406–2418.
20 Itohara S, Mombaerts P, Lafaille J, et al. T cell receptor delta gene mutant mice: independent generation of alpha beta T cells and programmed rearrangements of gamma delta TCR genes. *Cell*. 1993;72(3):337–348.
21 Nakae S, Komiyama Y, Nambu A, et al. Antigen-specific T cell sensitization is impaired in IL-17-deficient mice, causing suppression of allergic cellular and humoral responses. *Immunity*. 2002;17(3):375–387.
22 Lieschke GJ, Grail D, Hodgson G, et al. Mice lacking granulocyte colony-stimulating factor have chronic neutropenia, granulocyte

and macrophage progenitor cell deficiency, and impaired neutrophil mobilization. *Blood*. 1994;84(6):1737–1746.
23 Gottschalk TA, Vincent FB, Hoi AY, Hibbs ML. Granulocyte colony-stimulating factor is not pathogenic in lupus nephritis. *Immun Inflamm Dis*. 2021;9(3):758–770.
24 Chen N, Xie QM, Song SM, et al. Dexamethasone protects against asthma via regulating Hif-1alpha-glycolysis-lactate axis and protein lactylation. *Int Immunopharmacol*. 2024;131:111791.
25 Duan M, Li WC, Vlahos R, Maxwell MJ, Anderson GP, Hibbs ML. Distinct macrophage subpopulations characterize acute infection and chronic inflammatory lung disease. *J Immunol*. 2012;189(2):946–955.
26 Knudsen L, Weibel ER, Gundersen HJ, Weinstein FV, Ochs M. Assessment of air space size characteristics by intercept (chord) measurement: an accurate and efficient stereological approach. *J Appl Physiol*. 2010;108(2):412–421.
27 Wlodarska M, Thaiss Christoph A, Nowarski R, et al. NLRP6 inflammasome orchestrates the colonic host-microbial interface by regulating goblet cell mucus secretion. *Cell*. 2014;156(5):1045–1059.
28 Gottschalk TA, Hall P, Tsantikos E, L'Estrange-Stranieri E, Hickey MJ, Hibbs ML. Loss of CD11b accelerates lupus nephritis in lyn-deficient mice without disrupting glomerular leukocyte trafficking. *Front Immunol*. 2022;13:875359.
29 Godfrey DI, Zlotnik A. Control points in early T-cell development. *Immunol Today*. 1993;14(11):547–553.
30 Tan C, Taylor AA, Coburn MZ, Marino JH, Van De Wiele CJ, Teague TK. Ten-color flow cytometry reveals distinct patterns of expression of CD124 and CD126 by developing thymocytes. *BMC Immunol*. 2011;12:36.
31 Corbett AJ, Eckle SB, Birkinshaw RW, et al. T-cell activation by transitory neo-antigens derived from distinct microbial pathways. *Nature*. 2014;509(7500):361–365.
32 Matsuda JL, Naidenko OV, Gapin L, et al. Tracking the response of natural killer T cells to a glycolipid antigen using CD1d tetramers. *J Exp Med*. 2000;192(5):741–754.
33 Gherardin NA, Waldeck K, Caneborg A, et al. Gammadelta T cells in merkel cell carcinomas have a proinflammatory profile prognostic of patient survival. *Cancer Immunol Res*. 2021;9(6):612–623.
34 Guo XZ, Dash P, Calverley M, Tomchuck S, Dallas MH, Thomas PG. Rapid cloning, expression, and functional characterization of paired alphabeta and gammadelta T-cell receptor chains from single-cell analysis. *Mol Ther Methods Clin Dev*. 2016;3:15054.
35 Turner SJ, Diaz G, Cross R, Doherty PC. Analysis of clonotype distribution and persistence for an influenza virus-specific CD8+ T cell response. *Immunity*. 2003;18(4):549–559.
36 Tsantikos E, Gottschalk TA, L'Estrange-Stranieri E, et al. Enhanced Lyn activity causes severe, progressive emphysema and lung cancer. *Am J Respir Cell Mol Biol*. 2023;69(1):99–112.
37 Ramos FL, Krahnke JS, Kim V. Clinical issues of mucus accumulation in COPD. *Int J Chron Obstruct Pulmon Dis*. 2014;9:139–150.
38 Butler A, Walton GM, Sapey E. Neutrophilic inflammation in the pathogenesis of chronic obstructive pulmonary disease. *COPD*. 2018;15(4):392–404.
39 Barnes PJ. Inflammatory endotypes in COPD. *Allergy*. 2019;74(7):1249–1256.
40 Linden A, Laan M, Anderson GP. Neutrophils, interleukin-17A and lung disease. *Eur Respir J*. 2005;25(1):159–172.
41 Chen Y, Thai P, Zhao Y-H, Ho Y-S, DeSouza MM, Wu R. Stimulation of airway mucin gene expression by interleukin (IL)-17 through IL-6 paracrine/autocrine loop. *J Biol Chem*. 2003;278(19):17036–17043.
42 Gharib SA, Manicone AM, Parks WC. Matrix metalloproteinases in emphysema. *Matrix Biol*. 2018;73:34–51.
43 Sinha M, Lowell CA. Immune defense protein expression in highly purified mouse lung epithelial cells. *Am J Respir Cell Mol Biol*. 2016;54(6):802–813.
44 Ziegler SF, Marth JD, Lewis DB, Perlmutter RM. Novel protein-tyrosine kinase gene (hck) preferentially expressed in cells of hematopoietic origin. *Mol Cell Biol*. 1987;7(6):2276–2285.
45 Quintrell N, Lebo R, Varmus H, et al. Identification of a human gene (HCK) that encodes a protein-tyrosine kinase and is expressed in hemopoietic cells. *Mol Cell Biol*. 1987;7(6):2267–2275.
46 Ivanov II, McKenzie BS, Zhou L, et al. The orphan nuclear receptor RORgammat directs the differentiation program of proinflammatory IL-17+ T helper cells. *Cell*. 2006;126(6):1121–1133.
47 Cheng M, Hu S. Lung-resident γδ T cells and their roles in lung diseases. *Immunology*. 2017;151(4):375–384.
48 Paget C, Chow MT, Gherardin NA, et al. CD3bright signals on γδ T cells identify IL-17A-producing Vγ6Vδ1+ T cells. *Immunol Cell Biol*. 2015;93(2):198–212.
49 He JQ, Shumansky K, Connett JE, Anthonisen NR, Pare PD, Sandford AJ. Association of genetic variations in the CSF2 and CSF3 genes with lung function in smoking-induced COPD. *Eur Respir J*. 2008;32(1):25–34.
50 Aggarwal A, Baker CS, Evans TW, Haslam PL. G-CSF and IL-8 but not GM-CSF correlate with severity of pulmonary neutrophilia in acute respiratory distress syndrome. *Eur Respir J*. 2000;15(5):895–901.
51 Ashitani J, Mukae H, Taniguchi H, et al. Granulocyte-colony stimulating factor levels in bronchoalveolar lavage fluid from patients with idiopathic pulmonary fibrosis. *Thorax*. 1999;54(11):1015–1020.
52 Abboud MR, Taylor EC, Habib D, et al. Elevated serum and bronchoalveolar lavage fluid levels of interleukin 8 and granulocyte colony-stimulating factor associated with the acute chest syndrome in patients with sickle cell disease. *Br J Haematol*. 2000;111(2):482–490.
53 Wang H, FitzPatrick M, Wilson N, et al. CSF3R/CD114 mediates infection-dependent transition to severe asthma. *J Allergy Clin Immunol*. 2018;143(2):785–788.
54 Wickramasinghe LC, Tsantikos E, Kindt A, et al. Granulocyte colony-stimulating factor is a determinant of severe bronchopulmonary dysplasia and coincident retinopathy. *Am J Pathol*. 2023;193(12):2001–2016.
55 Newcomb DC, Boswell MG, Sherrill TP, et al. IL-17A induces signal transducers and activators of transcription-6-independent airway mucous cell metaplasia. *Am J Respir Cell Mol Biol*. 2013;48(6):711–716.
56 Fujisawa T, Chang MM, Velichko S, et al. NF-κB mediates IL-1β- and IL-17A-induced MUC5B expression in airway epithelial cells. *Am J Respir Cell Mol Biol*. 2011;45(2):246–252.
57 Fukuzaki S, Righetti RF, Santos TMd, et al. Preventive and therapeutic effect of anti-IL-17 in an experimental model of elastase-induced lung injury in C57Bl6 mice. *Am J Physiol Cell Physiol*. 2021;320(3):C341–C354.
58 Desai H, Marathe M, Potdar V, et al. An inhibitor of RORγ for chronic pulmonary obstructive disease treatment. *Sci Rep*. 2022;12(1):8744.
59 Eich A, Urban V, Jutel M, et al. A randomized, placebo-controlled phase 2 trial of CNTO 6785 in chronic obstructive pulmonary disease. *COPD*. 2017;14(5):476–483.
60 Singh D, Kolsum U, Brightling CE, Locantore N, Agusti A, Tal-Singer R. Eosinophilic inflammation in COPD: prevalence and clinical characteristics. *Eur Respir J*. 2014;44(6):1697–1700.
61 Heng TS, Painter MW. The immunological genome project: networks of gene expression in immune cells. *Nat Immunol*. 2008;9(10):1091–1094.
62 O'Brien RL, Roark CL, Born WK. IL-17-producing gammadelta T cells. *Eur J Immunol*. 2009;39(3):662–666.
63 Bozinovski S, Seow HJ, Chan SP, et al. Innate cellular sources of interleukin-17A regulate macrophage accumulation in cigarette-smoke-induced lung inflammation in mice. *Clin Sci (Lond)*. 2015;129(9):785–796.
64 Fujita T, Yoshioka K, Umezawa H, et al. Role of CD69 in the pathogenesis of elastase-induced pulmonary inflammation and emphysema. *Biochem Biophys Rep*. 2016;7:400–407.
65 Hong MJ, Gu BH, Madison MC, et al. Protective role of γδ T cells in cigarette smoke and influenza infection. *Mucosal Immunology*. 2018;11(3):894–908.
66 Urboniene D, Babusyte A, Lötvall J, Sakalauskas R, Sitkauskiene B. Distribution of γδ and other T-lymphocyte subsets in patients with chronic obstructive pulmonary disease and asthma. *Respir Med*. 2013;107(3):413–423.
67 Pons J, Sauleda J, Ferrer JM, et al. Blunted gamma delta T-lymphocyte response in chronic obstructive pulmonary disease. *Eur Respir J*. 2005;25(3):441–446.
68 Vargas-Rojas MI, Ramírez-Venegas A, Limón-Camacho L, Ochoa L, Hernández-Zenteno R, Sansores RH. Increase of Th17 cells in peripheral blood of patients with chronic obstructive pulmonary disease. *Respir Med*. 2011;105(11):1648–1654.

69 Freeman CM, Han MK, Martinez FJ, et al. Cytotoxic potential of lung CD8(+) T cells increases with chronic obstructive pulmonary disease severity and with in vitro stimulation by IL-18 or IL-15. *J Immunol*. 2010;184(11):6504–6513.

70 Chang Y, Nadigel J, Boulais N, et al. CD8 positive T cells express IL-17 in patients with chronic obstructive pulmonary disease. *Respir Res*. 2011;12(1):43.

71 Qiu W, Kang N, Wu Y, et al. Mucosal associated invariant T cells were activated and polarized toward Th17 in chronic obstructive pulmonary disease. *Front Immunol*. 2021;12:640455.

72 Constantinides MG, Link VM, Tamoutounour S, et al. MAIT cells are imprinted by the microbiota in early life and promote tissue repair. *Science*. 2019;366(6464):eaax6624.

73 Xu C, Li S, Fulford TS, et al. Expansion of MAIT cells in the combined absence of NKT and γδ-T cells. *Mucosal Immunol*. 2023;16(4):446–461.

74 Hassane M, Jouan Y, Creusat F, et al. Interleukin-7 protects against bacterial respiratory infection by promoting IL-17A-producing innate T-cell response. *Mucosal Immunol*. 2020;13(1):128–139.

75 Renne R, Brix A, Harkema J, et al. Proliferative and non-proliferative lesions of the rat and mouse respiratory tract. *Toxicol Pathol*. 2009;37(7 Suppl):5S–73S.

76 Lowell CA, Soriano P, Varmus HE. Functional overlap in the src gene family: inactivation of hck and fgr impairs natural immunity. *Genes Dev*. 1994;8(4):387–398.